NATIONAL AERONAUTICS AND SPACE ADMINISTRATION

Technical Report 32-1480

Solar Electric Propulsion System Tests

E. V. Pawlik
E. N. Costogue
J. D. Ferrera
T. W. Macie

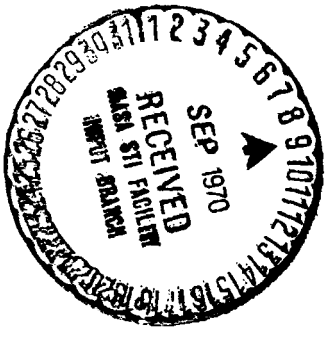

JET PROPULSION LABORATORY
CALIFORNIA INSTITUTE OF TECHNOLOGY
PASADENA, CALIFORNIA

August 15, 1970

NATIONAL AERONAUTICS AND SPACE ADMINISTRATION

Technical Report 32-1480

Solar Electric Propulsion System Tests

E. V. Pawlik
E. N. Costogue
J. D. Ferrera
T. W. Macie

JET PROPULSION LABORATORY
CALIFORNIA INSTITUTE OF TECHNOLOGY
PASADENA, CALIFORNIA

August 15, 1970

Prepared Under Contract No. NAS 7-100
National Aeronautics and Space Administration

Preface

The work described in this report was performed by the Propulsion Division with support from the Guidance and Control Division of the Jet Propulsion Laboratory.

Contents

Contents (contd)

Tables

Contents (contd)

Tables (contd)

Figures

Contents (contd)

Figures (contd)

Abstract

The design and experimental evaluation of a solar electric primary propulsion system is described. The system consists of two electron-bombardment ion thrusters complete with the associated thrust vector aligning actuators, a switching network, controller, and a flight-type power conditioner. The system was operated over a 2:1 range in output power. System integration problems such as matching of thruster performance and response to arcing within the thruster and solutions to these problems are described. Short endurance tests of the system were undertaken. Noise within the system was the major lifetime-limiting factor for both the power conditioner and controller.

Solar Electric Propulsion System Tests

I. Introduction

Solar-powered electric propulsion for use in interplanetary missions has been the subject of numerous reports (Refs. 1–3). In general, the mission advantages of solar electric propulsion appear to grow with the increasing mission difficulty. These advantages provide the impetus for more detailed investigations of this type of primary propulsion. A test program is under way at the Jet Propulsion Laboratory to examine in detail the system aspects of solar electric propulsion.

This report describes the design and testing of an electric propulsion system that incorporated the minimal features considered necessary for the primary propulsion system of a deep space probe. Most major elements necessary for a solar electric system were present. The system was essentially a breadboard arrangement that could form a baseline design for early electric propulsion flight systems. The objectives of these tests were to identify the problems associated with system integration and to develop solutions.

The capabilities of the system were:

(1) Closed-loop stable operation of a thruster (including a neutralizer) and a power conditioner.

(2) Remote control of thrust power over a 2:1 range by means of a single command signal (beam current reference signal).

(3) Remote starting and stopping of the power conditioner/thruster set.

(4) Remote reconnection of the power conditioner to a spare thruster.

(5) Automatic recycle after a sustained arc within the thruster.

(6) Single-axis thruster gimballing.

(7) Single-axis translation.

(8) Detection of a failure in the power conditioner/thruster set.

(9) Generation of the required telemetry data.

The system has been integrated and has undergone shakedown and some endurance testing. Some system test results have been previously documented (Refs. 4–8). All of the system test results are included in this report.

II. System Design

The propulsion system employed two 20-cm-diam electron-bombardment ion thrusters using mercury propellant. The propulsion system was designed to operate over a 2:1 range in output power to permit impedance matching to the solar array as the solar constant changes. All operation was at a fixed-nominal specific impulse of 4000 s. Each thruster was gimballed to provide ±10 deg of thrust vectoring about one axis. Therefore, when operated in pairs during flight, the thrusters can provide the necessary couple about the roll axis for attitude control. A cesium neutralizer was mounted on the support structure near each thruster. Thrusters, neutralizers, and gimbals were mounted on a common structure that could be translated along one axis. The thruster, neutralizer, and actuator portions of the system were mounted in a vacuum chamber. Photographs of the in-tank portion of this system are shown in Fig. 1. A schematic representation of the entire system is shown in Fig. 2.

A single, lightweight, modular power conditioning unit was employed. This unit, developed under contract by the Hughes Aircraft Company, was capable of operating either in atmosphere or in a thermal vacuum. Because of facility limitations, the operation tests for this program were in atmosphere only. A switching network allowed either thruster to be connected to the power conditioner or to laboratory power supplies. To minimize weight, all switching was accomplished with the power off. Failure of either the power conditioning unit or the ion thruster was detected by a failure logic system.

The system elements will each be described in detail. The weights of the elements used are presented in Table 1. These weights represent maximum values that can be reduced considerably in most cases.

Table 1. System weight breakdown

Component	Weight, g
Cathode transformer (each)	419
Gimbal actuator (each)	1,950
Latching valve	251
Neutralizer (each)	357
Power conditioning unit	14,969
Power conditioner cable and connectors	2,268
20-cm-diam ion thruster (each)	3,950
Thruster wiring and connectors (to connector bulkhead)	1,000
Structure (movable portion)	8,750
Switchgear (total of four)	2,945
Translator actuator	3,290
Controller (including failure logic)	1,800

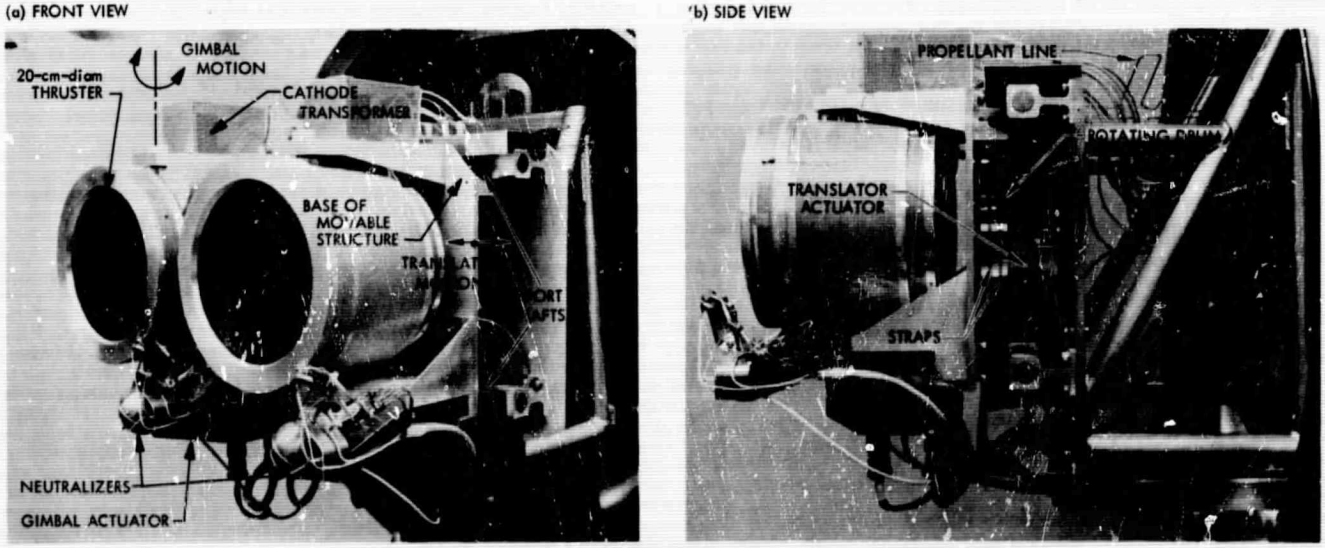

Fig. 1. In-tank portion of the propulsion system

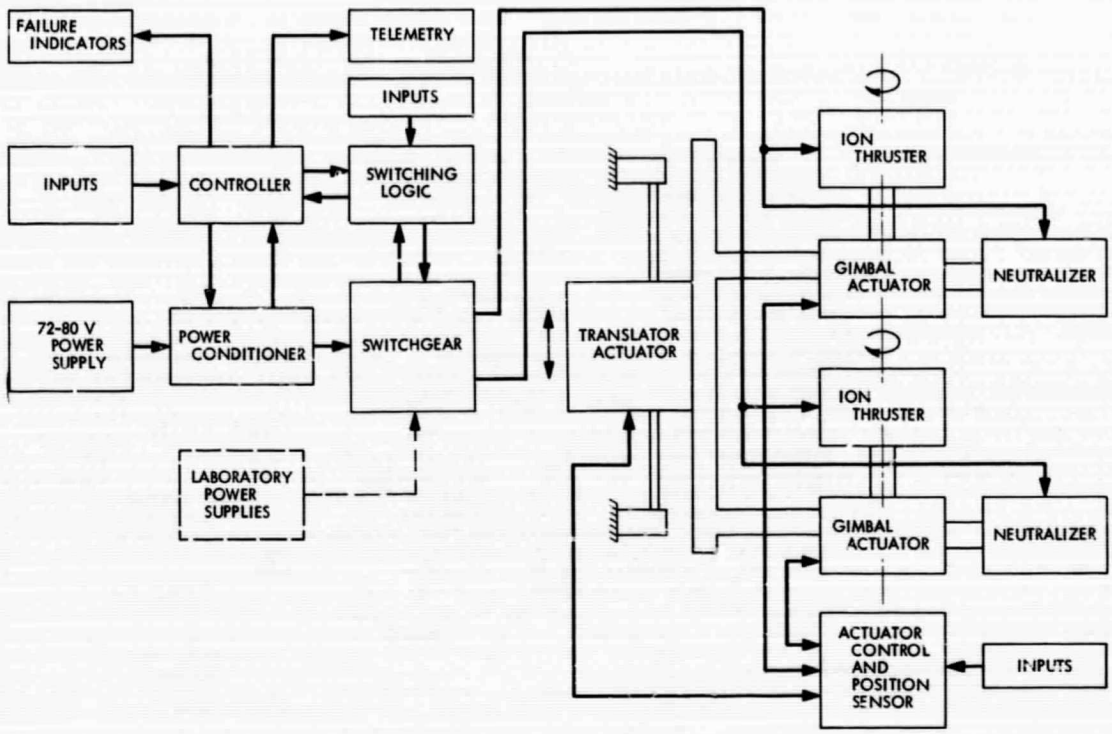

Fig. 2. Schematic diagram of solar electric propulsion system

A. Ion Thruster

The thruster configuration is shown in Fig. 3a. This 20-cm-diam thruster was designed to operate at a nominal input power of up to 2.5 kW, and with small modifications, it is the same thruster that is described in Ref. 9. A nominal net accelerating voltage of 2 kV was employed. Operation was normally maintained at near 90% propellant utilization, corresponding to a specific impulse of 4090 s. An ion beam current of 0.5–1.0 A was the normal operating region. The typical operating efficiency for this thruster is presented in Fig. 3b.

An oxide cathode was used for the electron source within the thruster. The selection of this cathode type was based on its availability and the knowledge of its characteristics. A hollow cathode (Ref. 10) now appears to be a more attractive selection for the primary electron source from the standpoint of both cathode power and lifetime, and will be used in future tests. The liquid mercury cathode (Ref. 11) is a possible second alternative that remains to be fully developed.

Tapered accelerator grids, as suggested in Ref. 12, were used on both thrusters. The grid thickness was decreased with the radial distance from the center of the grid in an attempt to increase the accelerator material in the region where the greatest wear is generally observed (Ref. 13). The center thickness was 0.30 cm and was constant to a radius of 5.0 cm from which it decreased to a thickness of 0.12 cm at the periphery. A weight saving of 150 g was thereby realized over grids with a 0.25-cm constant thickness.

The system used a functional relationship between the arc and beam currents to maintain a desired propellant utilization. This relationship was embodied within the power conditioning unit and required a high degree of quality control in the thruster construction. For this reason, considerable emphasis was given to the evaluation of the reproducibility of performance in a given thruster and to the duplication of performance from thruster to thruster.

An area that is very critical to reproducible thruster performance is the accelerating grid geometry. In an attempt to minimize thruster-to-thruster variability, prebowed screen grids, as described in Ref. 9, were initially used on both thrusters. Bench-checking of the grids, mounted on the thruster, was performed with dial indicators to measure grid movements as a heat gun and

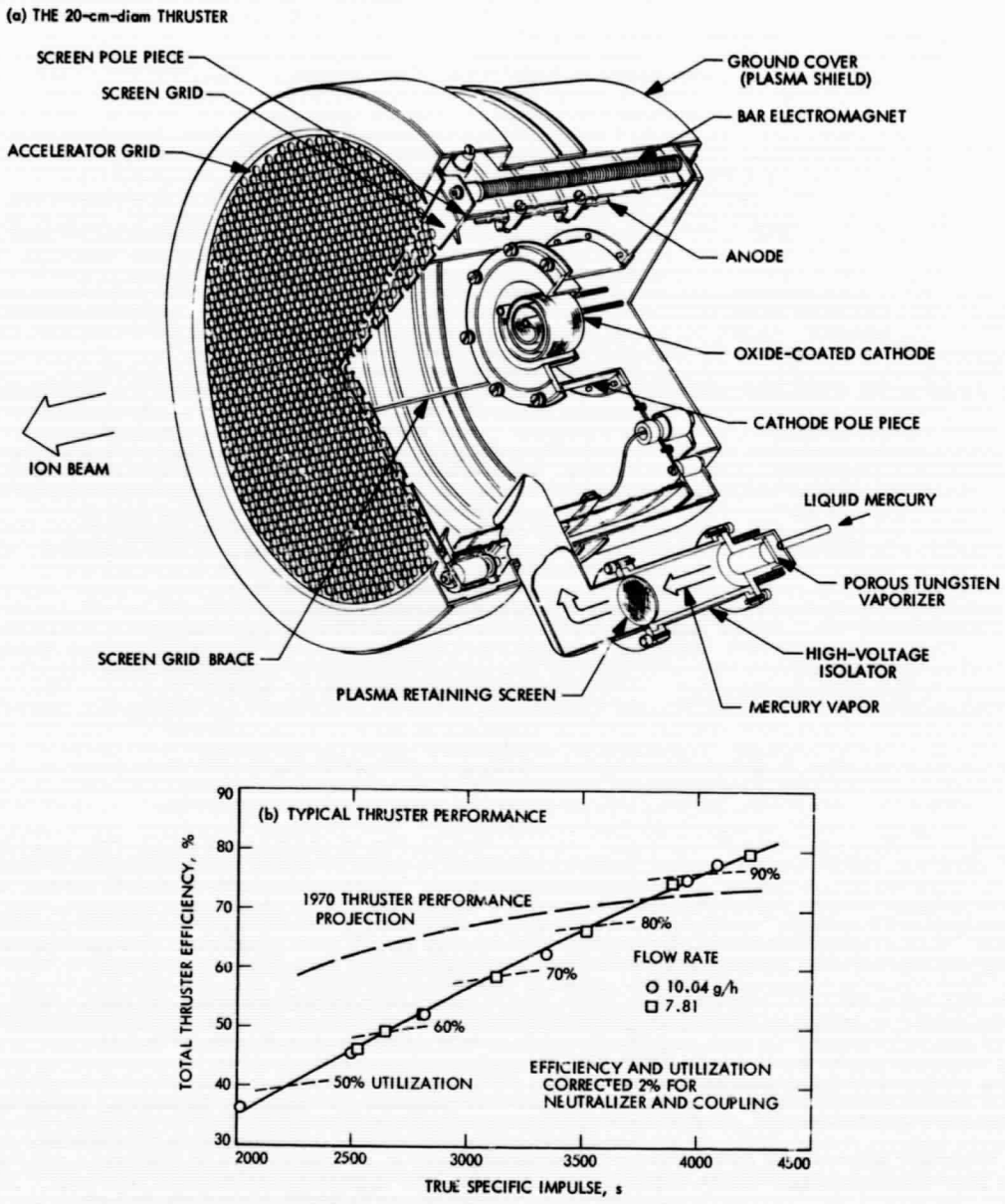

Fig. 3. The 20-cm-diam thruster

heat lamp served as plasma and cathode heat sources. These tests were performed on several screen grids, and the differences observed among the units are indicated in Table 2. Large variations in the nominal 0.175-cm spacing were observed as the thermal load was varied. The large differences and erratic results found with grid thermal loading were believed to be primarily because of inadequate stress relief during grid manufacture. In subsequent tests, however, carefully controlled stress relief was found to be inadequate to completely eliminate this problem.

In an attempt to reduce the grid geometry variations, with their attendant effects on ion chamber performance, thrusters using screen grid sets 1 and 3 were modified to include braces to restrict the screen grid movement (see Fig. 3). The braces were thin nonmagnetic stainless steel rods that tied the screen grid to the cathode pole piece. The results of bench tests, with the thruster using grids braced at one and at two locations, are included in Table 2. When a third brace was added, the screen grid exhibited little or no movement during bench thermal tests (less than 0.002 cm). This configuration, with three

Table 2. Ion thruster grid variations with thermal load

Grid set	Grid spacing variations from nominal, cm (nominal grid spacing 0.175 cm)		
	Heat on grid center, housing cold	Heat on grid and housing uniform	Heat on grid center, housing warm
1	−0.075	−0.015	−0.015
2	0.087	−0.005	−0.087
3	0.125	0.025	0.075
4	0.050	0.000	0.000
1 with one screen brace	−0.033	−0.005	−0.008
3 with two screen braces	0.012	−0.003	−0.003

symmetrical braces, was employed during all system testing.

B. Neutralizer

The Electro-Optical Systems cesium–plasma bridge neutralizer (Ref. 14) was included in the system. This type of neutralizer was chosen because at the time of selection it was the only available plasma bridge neutralizer that operated on an acceptably low propellant flow rate. Mercury-fed neutralizers might also have been used, but the types available required more propellant flow. Neutralizer selection for flight will be based on performance and on material interactions that are being considered in other work (Ref. 15).

The exact placement of the neutralizer with respect to the thruster is shown in Fig. 4. A cone half angle of 40 deg was assumed for the spread of the ion beam after leaving the thruster. This angle was determined for a similar thruster, reported in Ref. 16. The neutralizer was directed 45 deg downstream and was placed so as to be slightly removed from the beam edge. A distance of about 6 cm separated the neutralizer and the edge of the beam when the thruster was gimballed to the outermost position.

C. Mercury Feed

Mercury flow to the thrusters was from an external burette that permitted calibration of the vaporizers during thruster operation. The burettes were connected to a propellant reservoir by a latching solenoid valve. This latching valve requires power only during opening or closing, which makes it a desirable feed system feature to contain the mercury during launch. Incorporation of these devices in the test provided experience with their operation and reliability.

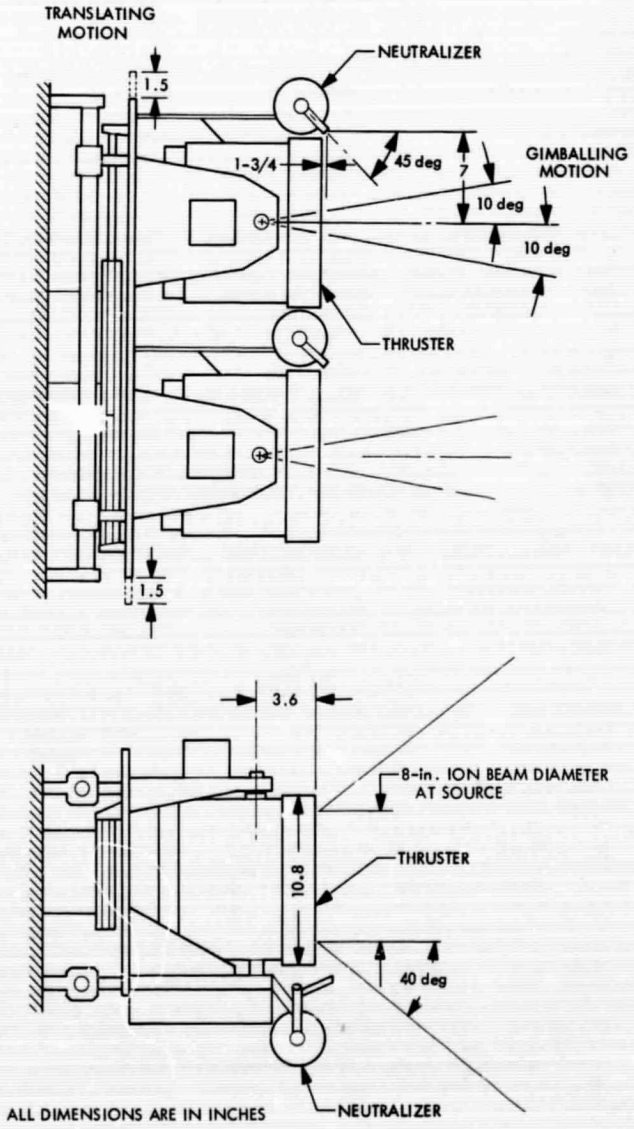

Fig. 4. Neutralizer position and translating motion

Stainless steel tubing, with 0.16-cm OD and 0.015-cm wall thickness, was used to connect the vaporizers to the burette. Each propellant feed line contained two loops 23 cm long to provide the necessary flexibility across the movable interface. This approach, while acceptable for a laboratory test, does not represent a solution for a flight system. Future tests using Teflon propellant lines are planned. This type of propellant line is felt to be more applicable to a flight system.

D. Power Conditioner

The power conditioning unit forms a vital link between the array of solar panels and the ion thruster and must meet three major requirements. First, the unit must convert the raw solar panel power into multiple dc and ac outputs required by the ion thruster. Second, it must provide the means of controlling and regulating the ion thruster according to specified thrust commands. Third, it must satisfy the requirements of low specific weight, high efficiency, and high-reliability operation. A power conditioner that was felt to be capable of meeting these criteria was procured from the Hughes Aircraft Company. This unit was modified from the unit reported in Ref. 17 and is shown in Fig. 5. Modifications included: (1) an increase in the total power level, (2) different control loops, (3) regulation of arc and magnet supplies, (4) incorporation of neutralizer power supplies, and (5) a redistribution of the power levels.

The interconnections between the ion thruster and the power conditioning unit are shown in Fig. 6. The outputs of the individual power supplies are listed in Table 3 and are broken into two groups to aid in identifying the turn-on sequence. The power conditioner delivered a nominal power of approximately 2450 W, while the maximum power handling capacity was 2800 W. The input power was delivered at a voltage that could range from 72 to 80 Vdc. The unit weighed 38 lb (includ-

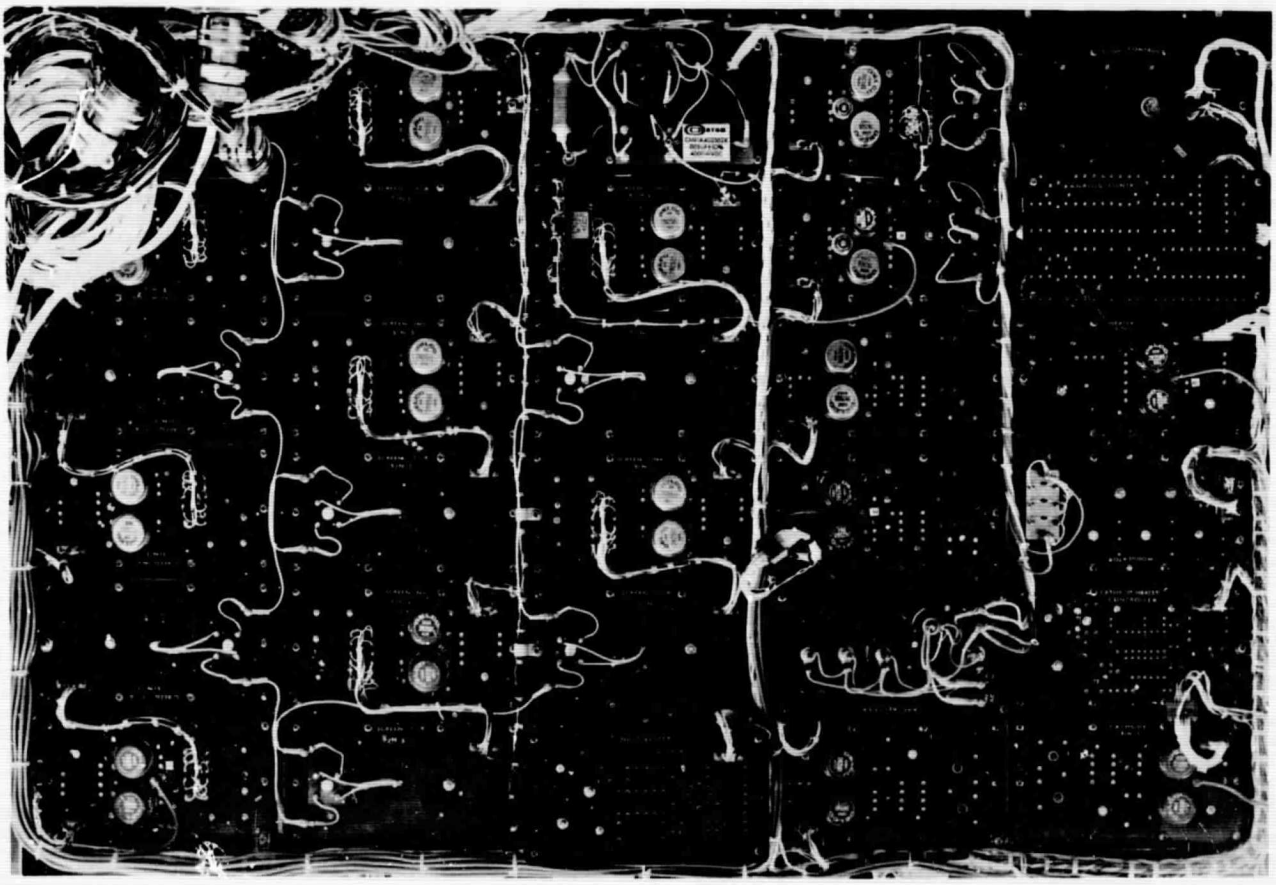

Fig. 5. Power conditioner, radiating side

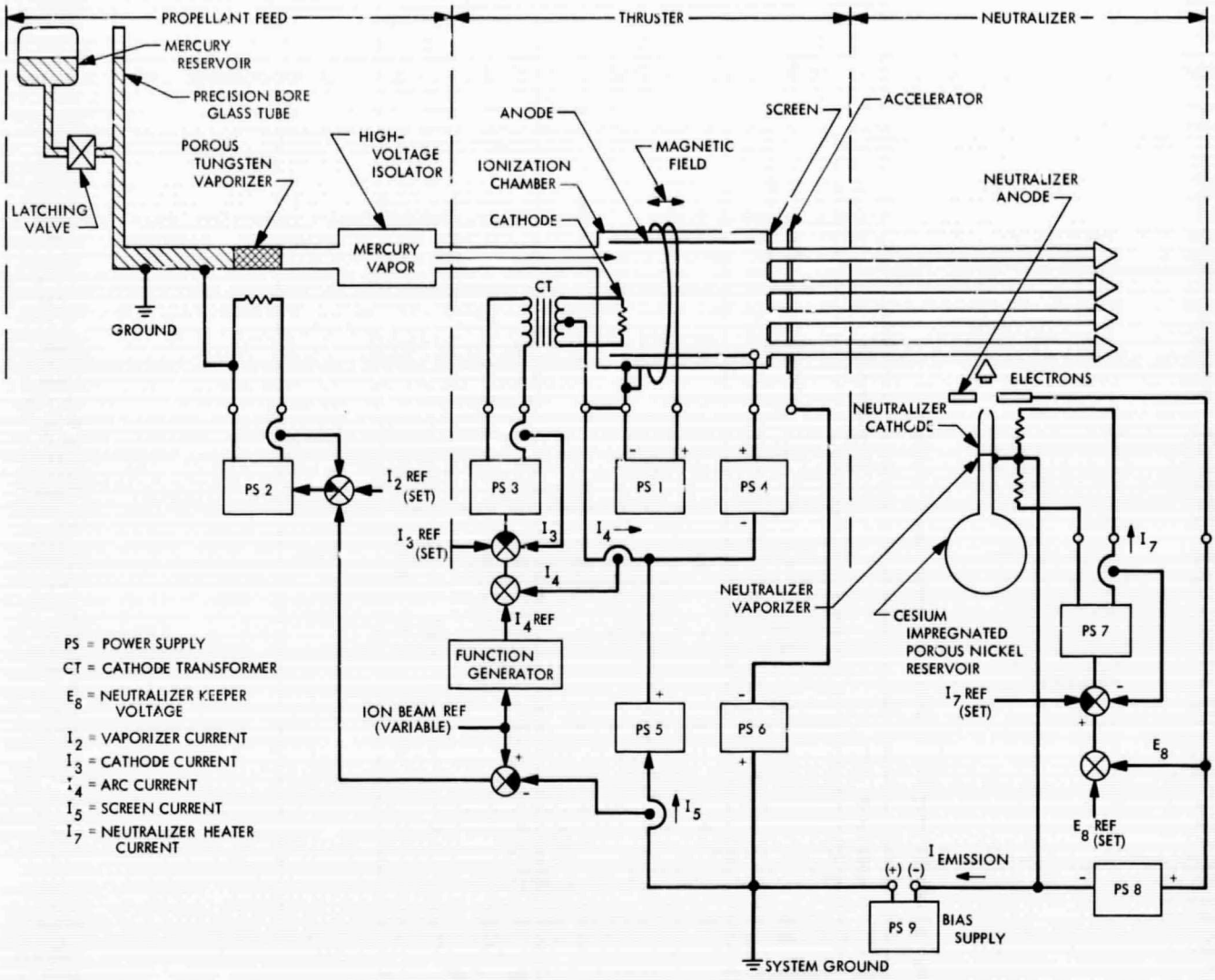

Fig. 6. Electrical connections for the power conditioner and thruster

ing approximately 5 lb for cables and connectors) and its dimensions were 25¼ × 37 × 6 in. It consisted of 30 individual modules, including redundant units, mounted on a supporting frame. The efficiency, as measured by panel meters, was 90%. While this weight and efficiency at this power level were considerably better than any previously reported, it is felt that improvements are possible. Attempts were not made to minimize the weight or to maximize the efficiency during this phase of the program. A power conditioner is presently being developed under contract by Hughes Aircraft Company that will operate at the same power level, but with a lower weight and higher efficiency. In addition, other system requirements such as a variable input voltage and closer voltage regulation will be included.

The advantages of the modular concept used in the power conditioner are well known (Refs. 18–20). The low specific weight of the modular system is attributed to the fact that the individual modules operate at low power levels, for which high-frequency transistors are available. Most of the inverters operate at 12 kHz (compared, for example, with 8 kHz for SERT II), which reduces the size and weight of all the magnetic components.

High efficiency is also possible because the individual components are operated at low specific stress so the losses in all the semiconductors and magnetics are very low. The low power dissipation of each module eliminates the need of additional heatsinks or radiators as the mounting chassis is large enough to dissipate all the losses by

Table 3. Ratings of power supplies within the power conditioning unit

Group	No.	Supply	Type	Output[a]	Maximum ratings[b]			Nominal ratings					Range of control
					E, V	*I*, A	I_{11m}, A	*E*, V	*I*, A	*P*, W	Peak ripple, %	Load regulation of output voltage, %	
I	1	Magnet manifold heater	dc	F	19	0.85	0.90	15	0.67	10.5	3.5	—	—
	3	Cathode heater	ac	V	5	40	45	45	35	160	—	—	10–10 A
	7	Neutralizer heater	ac	V	12	3.4	4	12	2.8	35	—	—	0.3–3.4 A
	8	Neutralizer keeper	dc	F	300 V 5 mA	20 mA 95 V	0.55	10	0.50	5	5 at 10 V	1.0	0.02–0.5 A
II	2	Vaporizer	ac	V	10	2	2.05	5.5	1.1	6	—	—	0.5–1.2 A
	4	Arc	dc	V	150 V	7 at 35 V	8	34.5	6	207	1.25	2.2	2–7 V
	5	Screen	dc	V	2260[c]	1.0	1.05	1980	1.0	2000	3.8	4.4	0.5–1.0 A
	6	Accelerator	dc	F	2710[c]	0.11	0.115	2170	0.005	11	2	5.8	—

[a]Output: V = variable, F = fixed.
[b]At an input voltage of 80 V.
[c]At no load.

direct radiation to space. The low specific weight of all the individual components makes the mounting and supporting structure very light. In addition, the reliability of power semiconductors is improved because of the lower operating temperatures obtainable by using the modular approach.

The multimodule system also offers greater flexibility in the use of the individual outputs during system turn-on by allowing a sequencing of the modules, and, in case of failure, by switching to a spare module.

Table 4 lists both the working and spare modules. Changeover from the working to spare module was performed electronically by means of a command generated by an internal failure logic. No significant interruption in the thruster operation was observed to result. The main building blocks are shown in the diagram presented in Fig. 7. Each power supply will be described in turn.

1. Accelerator power supply (supply 6). The accelerator power supply consisted of two power converters. One converter was operational and the other was a standby. Each converter consisted of a free-running inverter that operated at approximately 12 kHz, followed by a transformer–rectifier combination. The dc outputs of the two units were connected in series. The output transformer of the inverter was equipped with an additional ac winding, used to synchronize the screen and arc inverters. The dc output from the accelerator converter was filtered to reduce the 24-kHz ripple to an acceptable level.

2. Screen power supply (supply 5). Eight identical converters were provided to make up the screen power supply. Each consisted of a single-phase, unregulated, driven power inverter followed by a transformer–rectifier stage. On the input side, all of the converters were connected in parallel and fed from a single dc source. On the output side, the individual dc outputs were connected in series.

Seven converters were used to deliver the beam power. The eighth converter served as a spare. A filter was used to reduce the dc ripple of the output to an acceptable level.

3. Arc power supply (supply 4). The arc power supply contained two identical inverters connected in parallel.

Table 4. Power conditioner modules

Power supply		Inverters	
No.	Description	Working	Spare
1, 2, 7, 8	5-kHz subsystem	1	1
3	Cathode	1	1
4	Arc	1	1
5	Screen	7	1
6	Accelerator	1	1

One was operational, the other a standby. Regulated arc inverters were used since a load regulation of 1½% was desired for this power supply because of the sensitivity of propellant utilization control. Regulation was accomplished by pulse width modulation while the frequency remained constant at 12 kHz. The ac output of the inverter in use was connected through a relay to an output rectifier and filter. It should be noted that an unusual volt/ampere output characteristic was required since a higher arc voltage is needed to initiate the arc. This dual characteristic was obtained by using two rectifier bridge outputs connected in parallel.

4. The 5-kHz subsystem. The 5-kHz subsystem consisted of four power supplies: (1) neutralizer keeper (supply 8), (2) magnet manifold heater (supply 1), (3) vaporizer (supply 2), and (4) neutralizer heaters (supply 7). A common preregulator that reduced the voltage level from the approximate 80 to 40 V was employed. This regulator feeds two inverters connected in parallel. One of the inverters is used as a spare.

The inverters were of a free-running type that generated 5-kHz square-wave power. This ac power was divided into the following four parallel branches:

(1) Neutralizer keeper power supply (supply 8). The dual volt/ampere characteristic required for this supply was similar to that of the arc power supply, although the two dc outputs were in series, rather than parallel. The output was filtered.

(2) Magnet manifold heater power supply (supply 1). An ac magamp regulator was used to control the output; the transformer–rectifier followed, converting ac to dc. The use of the transformer was required in order to isolate the primary, which operates at ground potential, and the output, which floats at the screen potential (2 kV).

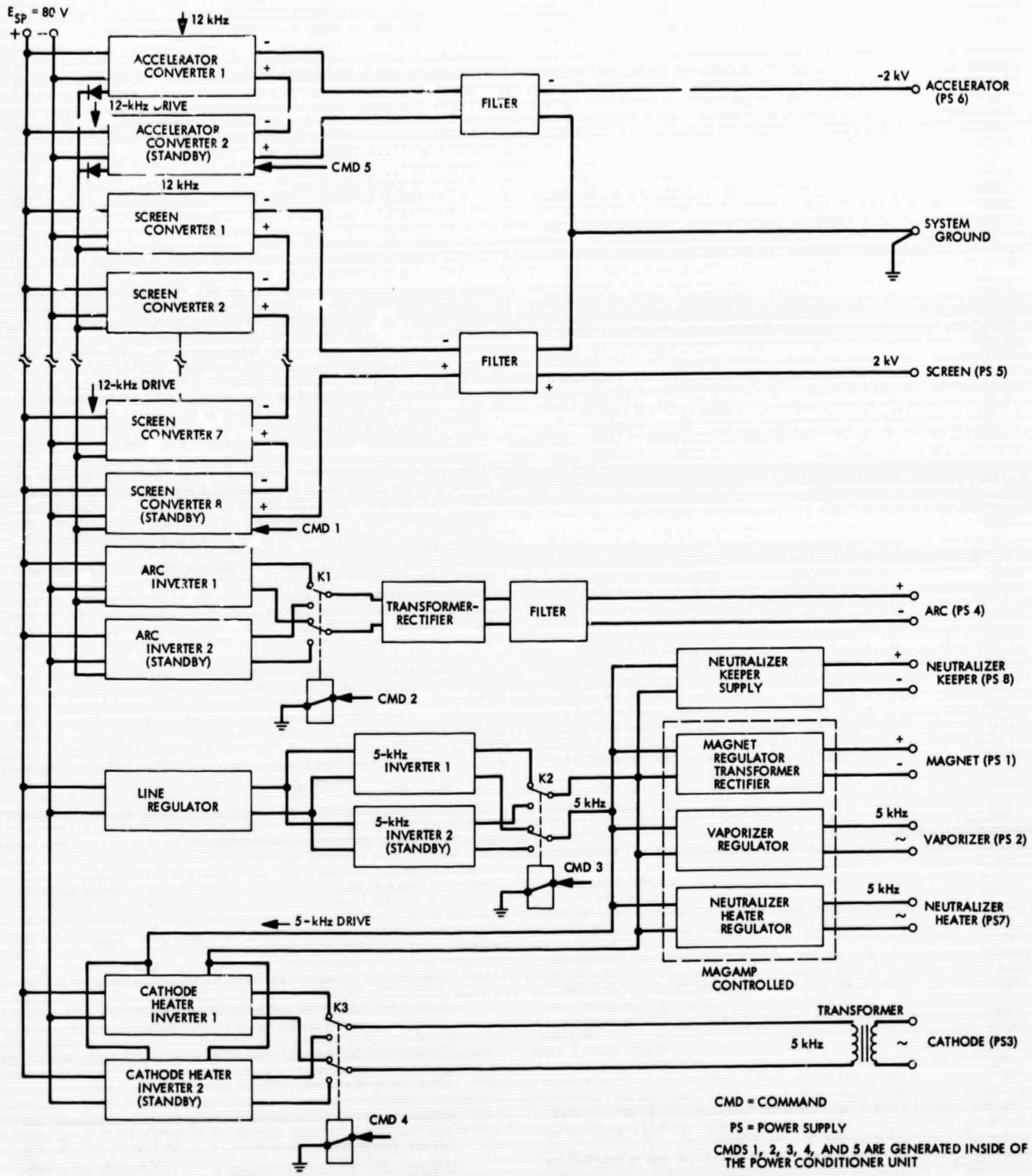

Fig. 7. Block diagram of power conditioner

(3) Vaporizer power supply (supply 2). This supply was an ac magamp regulator delivering 5-kHz square-wave power to the heater.

(4) Neutralizer vaporizer and cathode heaters (supply 7). This supply was similar to the vaporizer supply.

5. Cathode heater power supply (supply 3). Two identical power inverters were available to make up the cathode heater power supply in order to provide the desired redundancy. The inverters were a driven type, regulated, and operated at a constant frequency of 5 kHz. The output power could be varied by changing the duty cycle. The output transformer was located remotely, in the vicinity of the thruster. This served to reduce the transmission losses and to improve regulation.

6. External controls. The power conditioner was provided with remote control to: (1) start the system, (2) regulate the level of power delivered to the thruster, and (3) shut down the system.

a. Startup. Table 3 shows the individual power supplies arranged in two groups. Group I was turned on first; group II followed after a delay of approximately 15 min. The first 15 min was used to preheat the oxide cathode and the manifold, establish the magnetic field around the thruster, and start the neutralizer. After group II was energized and the arc initiated, the thruster would begin to generate thrust; the magnitude of thrust would build up slowly until after the thruster achieved thermal equilibrium and it reached the final desired level. From this point, the thrust would be regulated according to the mission profile.

b. Ion beam control. The beam current expelled by the thruster must be decreased with time, since less power will normally be available from the solar array during a mission in which the distance from the sun increases. The beam current was regulated by means of a remote analog signal. A variation of the reference voltage that ranges from 0 to 5 Vdc linearly changed the ion beam current from 0.5 to 1.0 A.

c. Shutdown. Two methods of shutdown were available. The first one consisted of turning off all of the power supplies at the same time. The second one, to minimize the possibility of condensation of mercury on thruster surfaces, initially turned off only the vaporizer supply. As the delivery rate of mercury vapor decayed, the ion beam density started to drop. When the value of ion beam current dropped to one-third of the original level, another remote command turned off the power conditioning unit.

7. Self-protection. All power supplies were short-circuit proof and would not be damaged if an overload occurred. Excessive currents to the arc, accelerator, or screen supplies would cause all group II power supplies to shut down and restart a short time later (initially on the order of 1 s).

8. Servo loops. Three distinct servo loops were provided and can be identified in Fig. 6. These are: (1) the neutralizer loop, consisting of supplies 7 and 8, (2) the beam current loop, consisting of supplies 5 and 2, and (3) the cathode–arc current loop, consisting of supplies 3 and 4.

The first loop was closed as soon as the neutralizer was started. The second and third loops were closed only after the plasma in an operating thruster was established. A block diagram of the control loops for the ion thruster is presented in Fig. 8. These control loops have been analyzed and are discussed in Ref. 21. The main conclusions for the analytical model used are that the loops are stable under most operating conditions. The need to control the propellant utilization accurately imposes tight (1% or better) output regulation requirements on the power conditioner. It was also found that operation at high propellant utilization (90% or better) eased this requirement slightly.

9. Telemetry. The power conditioning unit had special outputs suitable as inputs to a decoder. All parameters that were considered essential for determining the power functioning of the ion thruster were available for transmission. Table 5 lists the parameters that were provided. These currents and voltages are translated into 0–5 Vdc analog signals. Certain of these signals also served as inputs to the failure detection circuitry.

E. Switching Matrix

The power conditioning unit could be linked to either of the two ion thrusters by means of multiple-contact, multiple-deck selector switches. A photograph of the four switches used is shown in Fig. 9. These switches were intended for laboratory use in atmosphere only. Lightweight, sealed units would be necessary for flight applications. Each switch contained four decks with two poles per deck and six positions per pole. Each pole was

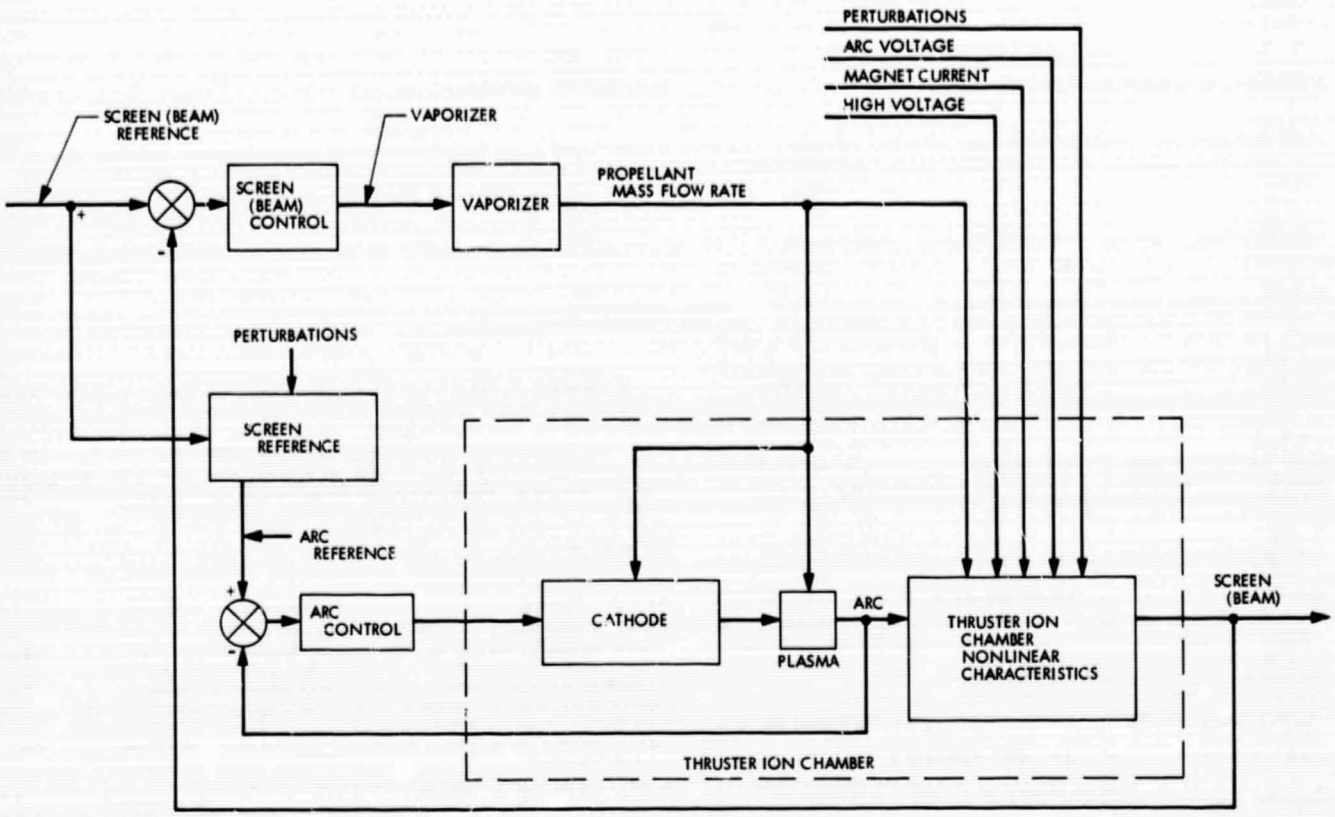

Fig. 8. Block diagram of thruster control loops

capable of carrying 8 A. Voltages up to 4 kV could be applied between contacts. The design permitted switching only when the power conditioner was turned off. Two such switches were required per power conditioning unit. The four switches that were used in the system also permitted the laboratory power supplies to be connected to either thruster. Excess capacity existed within this system for connections to as many as four additional ion thrusters.

The switchgear was operated by a remote control unit equipped with switching logic to permit the specification of thruster and power conditioner combination. Switching occurred upon a manual command. Lights were used to indicate the switch status. The electronic circuitry provided the required interlocks inhibiting switching when the power conditioner was energized and provided a signal to the controller that prevented operation of the power conditioner if the switching operation malfunctioned and allowed more than one thruster to be connected to a power conditioner, or more than one power conditioner (laboratory power supplies and power conditioning unit) to be connected to one thruster. A more detailed description of the switchgear and switchgear logic is given in Ref. 22.

F. Controller and External Failure Logic

The controller and external failure logic unit served to: (1) provide command signals to the power conditioning unit, (2) monitor telemetry outputs, (3) detect a failure of either the ion thruster or power conditioning unit, and (4) inform switchgear logic when the power conditioner was on. In providing the command signals, it sequences the starting of the system, generating a preconditioning sequence for the cathode and neutralizer. It also specifies the level of the ion beam power. A logical extension of this unit would be, upon detecting failures, to direct the operation of the switchgear.

The failure detection unit monitored only the ion beam current and the screen and accelerator voltages. A failure was defined as a deviation of any of these parameters greater than $\pm 10\%$ of their specified values. Since most failures that could occur within the system resulted in either no ion beam current or a value greatly different

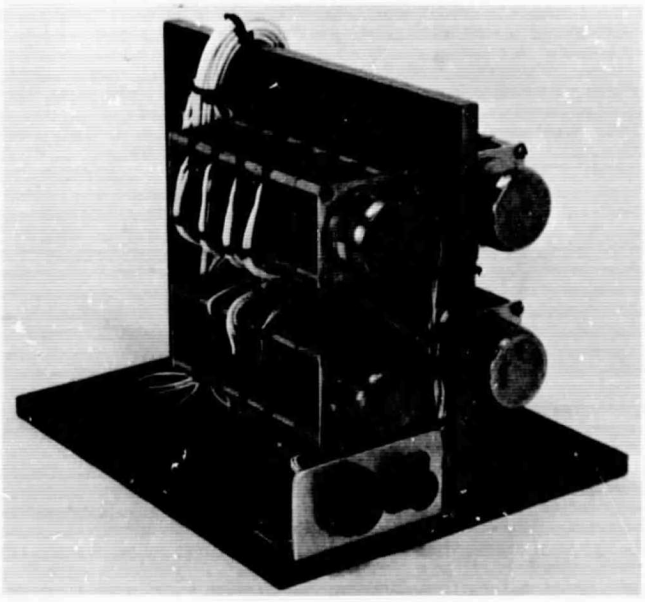

Fig. 9. Switchgear

from that desired, this simple failure detection scheme was felt to be adequate. Measured parameters must remain outside of the acceptable range for a longer duration than 3 s (initial setting) for this unit to register a failure.

The ion beam current level during system operation was variable since: (1) the steady-state value could be specified within a 2:1 range, and (2) the initial thruster turn-on retards the ion beam from reaching the lower limits of its operating range because of the long thermal time constant of the ion thruster. For this latter reason, the controller must time-sequence the turn-on of the beam failure detection. The lower limit of the failure monitor is initially zero after thruster turn-on and is increased incrementally in each of the next three 30-min periods.

The assigned functions of the failure logic system were performed by means of commercially available micrologic cards. This approach facilitated rapid changes and modifications that greatly reduced the development effort associated with this unit but did not represent an attempt to minimize the controller weight. These logic cards are included in Table 1 in the controller weight.

G. Thrust Vector Control

The thrust vector control consisted of the actuators and control electronics. This part of the system was

Table 5. Power conditioner telemetry outputs

Power supply	Name	5-Vdc signal corresponds to	
		Current, A	Voltage, V
1	Magnet manifold	0.9	—
2	Vaporizer	2.2	—
3	Cathode	40.0	—
4	Arc	8.0	40
5	Screen	1.0	2000
6	Accelerator	0.020	2000
7	Neutralizer heaters	4.0	—
8	Neutralizer keeper	1.0	30

constructed to demonstrate proof of concept regarding precision, reliability, and system compatibility. Flight environment and weight requirements were given secondary attention. The mounting of the gimbal and translator actuators on the in-tank portion of the propulsion system is shown in Fig. 1. The initial breadboard work is described in Ref. 6.

Briefly, the thrusters are gimballed ±10 deg, which is adequate to provide a couple about the roll axis for attitude control. During the powered portion of the flight, translation in two orthogonal directions provides: (1) the capability of positioning the resultant thrust vector through the center of gravity of the spacecraft as successive thrusters are shut down because of power limitations, and (2) pitch and yaw for attitude control. Many gimballing and translation mechanisms were studied in the early phases of this program. The two that were picked as the best candidate designs are discussed in the subsequent paragraphs.

1. Gimbal actuator. The characteristics of the gimbal actuator are listed in Table 6, and the actuator is shown in Fig. 10. The unique feature of this actuator was the drive arrangement used to minimize backlash between the output shaft and feedback pickoff in order to obtain the design goal of 0.1 mrad (20.6 arc s) of shaft rotation per stepper motor step input.

The linear motion of the saddle nut due to the lead screw was transformed to the rotary motion of the output sector through two beryllium copper straps. The saddle nut was also pinched slightly prior to machining of screw threads such that, in its assembled state, the saddle nut

Table 6. Actuator characteristics

Parameter	Gimbal actuator	Translator actuator
Output travel, in.	—	±3
Output travel, deg	±10	—
Nominal stepping rate, steps/s	50	100
Actuator slewing rate, in./s	—	0.025
Actuator slewing rate, mrad/s	5	—
Temperature range, °F	−50 to +275	−50 to +275
Resolution, in./step	—	0.0025
Resolution, arc s/step	20	—
Backlash, arc s	0	5
Gear train ratio	15708:1	2930:1
Power required, W	7	7
Output torque at nominal rate, in.-lb	55	50
Weight, lb	4.3	7.25
Leak rate (90% nitrogen, 10% helium), cm^3/h	0.005	0.005
Pickoff scale factor, V/deg	—	0.14
Pickoff scale factor, V/in.	12.55	—
Pickoff linearity, %	0.14 (full scale)	0.5
Excitation, Vdc	24	±24

screw threads were forced into contact with the lead screw threads. A solid rod connected the saddle nut to the pickoff arm. Thus, there was essentially zero backlash between the actuator output shaft and the position pickoff. The position pickoff was a linear, variable-differential transformer that sensed lead screw position. Total pickoff arm travel was approximately ±1.5 cm, corresponding to ±10 deg of travel of the output sector.

The drive motors in both actuators were size 11, 90-deg, permanent-magnet stepper motors. The nominal input stepping rate for the gimbal actuators was 50 steps/s although, in actual flight use, the rate could be as low as one step over a period of hours. The gear train ratio provided 0.1 mrad output rotation per stepper motor input step. Aside from the backlash problem, one of the main areas of concern in designing the actuator was the thermal environment that the actuator components would see. This concern arose because of their proximity to the thrusters whose maximum operating temperature was on the order of 250°C. A detailed thermal analysis was performed that resulted in making an intermediate

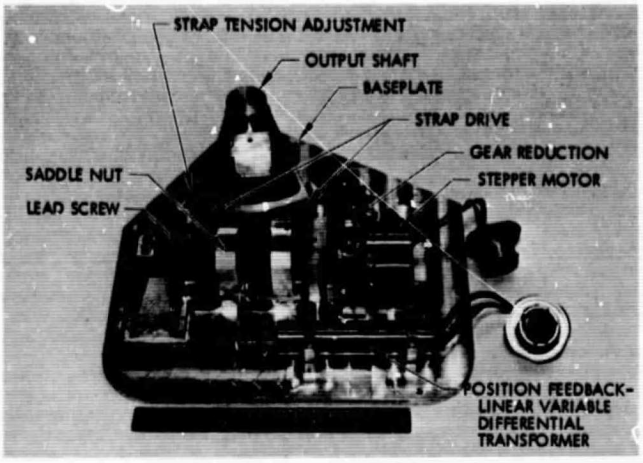

Fig. 10. Internal view of gimbal actuator

shaft connecting the actuator to the ion thruster of stainless steel, rather than aluminum, to minimize heat transfer to the actuators. With the exception of the straps, all parts of the actuator were made of aluminum. The lead screw itself was a hollow aluminum shaft, hard-anodized after machining. For the system testing of the actuator, six thermistors were attached internally to monitor temperature during thruster operation. The actuator case was a sealed unit and is pressurized to 5 psia using a 90% N, 10% He mixture. Static seals were provided by a single O-ring. The dynamic output shaft seal was accomplished by using two O-rings separated by a lubrication groove. The output shaft was supported prior to its attachment to the thruster by a bronze sleeve bushing. Mechanical stops were provided inside the actuator to limit mechanical travel to ±12 deg.

2. Translator actuator. The characteristics of the translator actuator are also listed in Table 6, and the actuator is shown in Fig. 11. Two features are particularly noteworthy. The first is the application of a harmonic drive gear train to obtain very low values of backlash (less than 5 arc s) and high output torsional stiffness. This item can be purchased as off-the-shelf hardware with the low level of backlash specified. This low backlash is obtained by the vendor through careful selection and matching of component parts. The second noteworthy feature is the platform drive external to the actuator. This motion was accomplished by the use of a flat-strap type of drive that connects the output drum to stainless steel roller bearings that ride on parallel stainless steel shafts. Fatigue cracks that might develop in the strap drive are self-healing in a space vacuum. It is anticipated that ceramic balls will be used in the roller bearings to eliminate the possibility of cold welding of similar metals

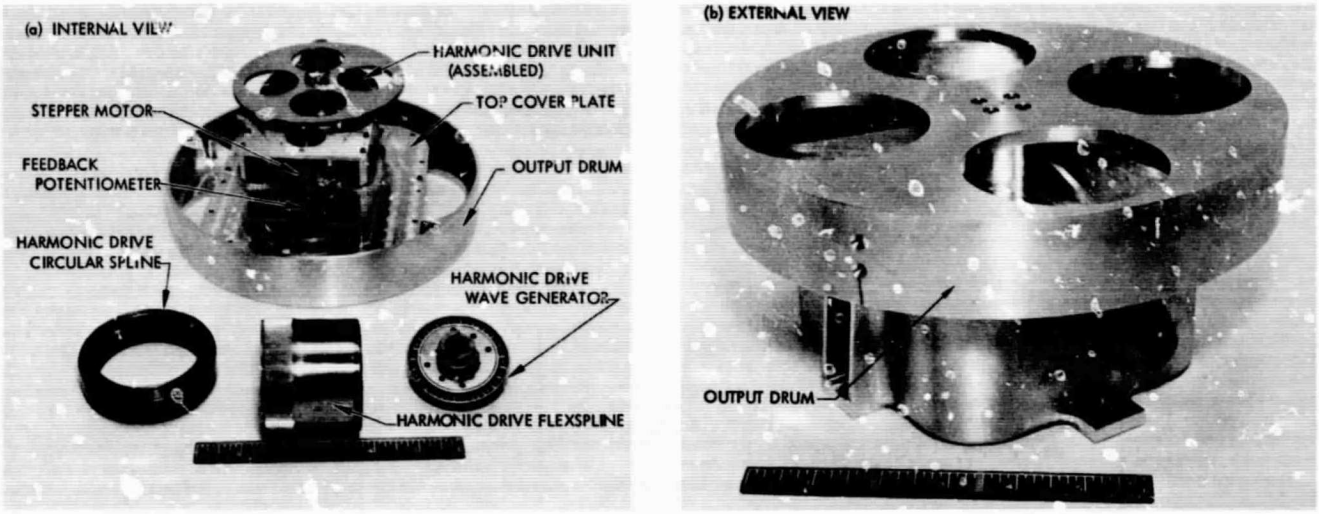

Fig. 11. Translator actuator

in a space vacuum. Mechanical stops on the stainless steel rods limited mechanical travel to ±7.5 cm for the system tested. The system was capable of 33 cm of travel when removed from the vacuum chamber. As mentioned previously, a size 11 stepper motor was used. The gear ratio provides 0.0064 cm (0.0025 in.) of output translation per stepper motor step. A rotary infinite resolution potentiometer was used for position feedback. Mechanical feedback gain is approximately 1. As mentioned for the gimbal actuator, similar metals were used here also to minimize thermal expansion problems. This actuator was also instrumented with thermistors to provide temperature feedback information during system testing.

3. Thrust vector control electronics. A thrust vector control unit provided open-loop actuator control and test instrumentation. A simplified block diagram of the electronics is shown in Fig. 12. Operation of only one gimbal or the translator actuator at a time was permitted. Stepper motor speed rates of 5, 50, or 100 steps/s, in addition to single-step operation, were available. An electronic counter was used to count the number of pulses to the stepper motor. The three-position outputs can be read simultaneously from meters, or individually at higher accuracy by using a digital voltmeter or digital printer. Signal conditioning of the pickoff output signals was provided to: (1) filter noise, and (2) maintain a constant load on the transducers.

A mode selector switch allowed for two types of operations. In the test mode, with the stepper motor energized, the actuator would run until the pickoff voltage reached a set level (corresponding to slightly less than design mechanical travel) and then was stopped electronically. During the run mode, the polarity of the voltage supplied to the stepper motor was automatically reversed when the electrical stop was reached. The motor would then drive in the opposite direction. The run mode was intended primarily for endurance testing.

H. Mounting Structure

An aluminum structure was used to mount the ion thrusters, gimbal actuators, translator actuator, cathode transformers, and neutralizers. The construction consisted mainly of thick, flat members, providing a rigid structure. All removable support arms were pinned to provide accurate alignment during assembly. No attempts were made to minimize the structure weight.

III. Instrumentation

In order to interpret and accurately evaluate system performance, all relevant parameters were recorded. Thermocouples and thermistors at locations shown in Table 7 provided data on temperatures. All electrical parameters (Table 8) were either displayed on 2% accuracy instruments or recorded on strip charts, magnetic tapes, and digital printouts. The indicating instruments were used to gather information on the steady-state operation of the system; the readings were thoroughly recorded in laboratory records and used for mapping and performance evaluation. The pen-type strip chart recorders provided graphical records of the individual channels and permitted continuous monitoring of the system behavior.

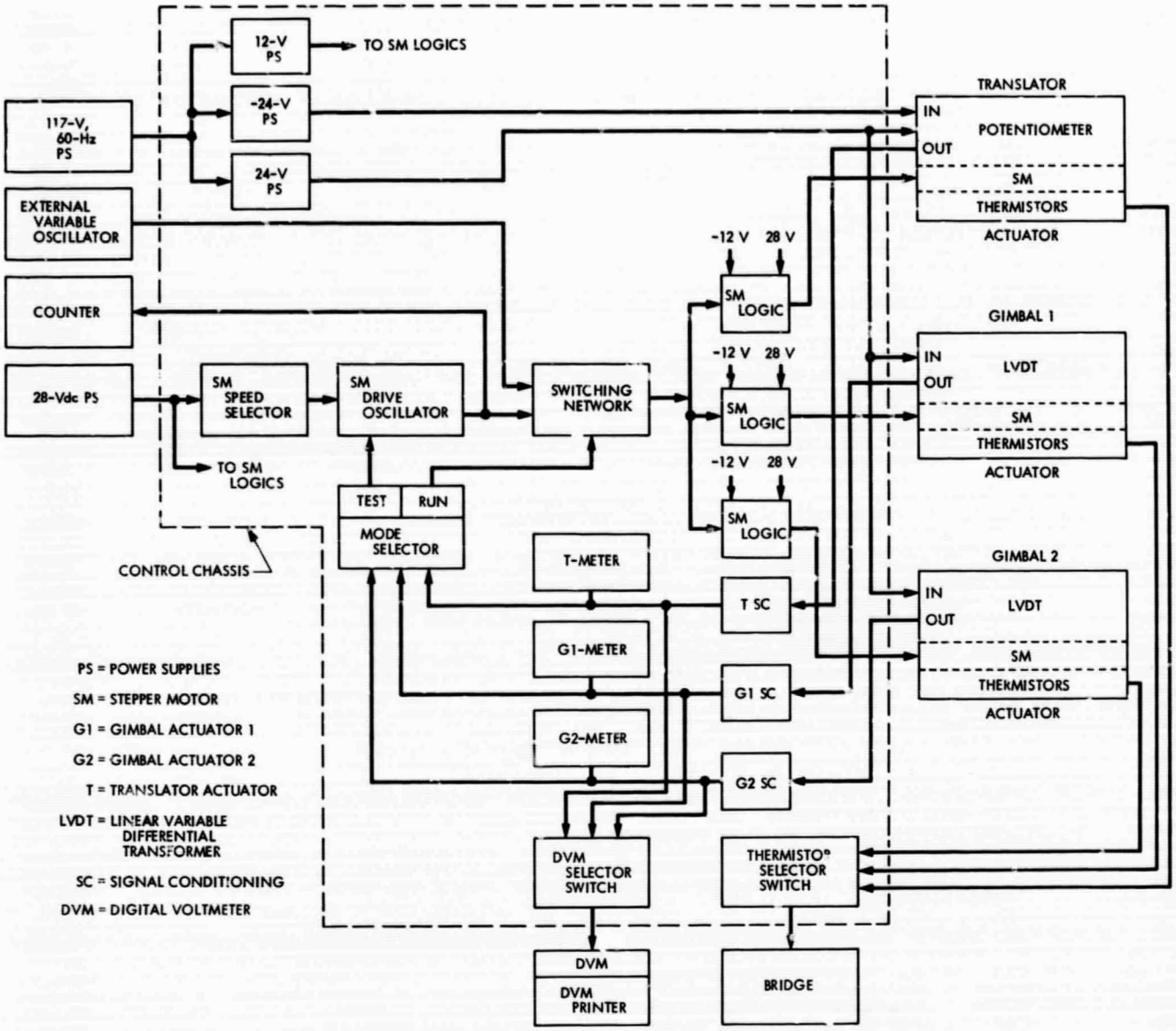

Fig. 12. Block diagram of thrust vector control electronics

To gather detailed transient data during thruster arcing, system shutdowns, and system recovery, a 14-channel analog acquistion system using magnetic tape was used for recording. Twelve channels were employed for acquisition of electrical parameters; the other two were used for recording NASA time and the voice of the test engineer.

In the analog acquisition system, the analog signals were first magnetically recorded in the FM mode. Subsequently, the playback system translated the FM signals into light signals that were transferred to a photosensitive paper tape. Any desired resolution within a range of 0.16–160 in./s was available, with the possibility of an additional expansion of this range by means of slowing down or speeding up of the original data tape as recorded.

The form of the tripping signals, as generated by arcing, could also be observed on a memory oscilloscope. The microsecond-type interference that penetrated the electronics was measured by a memory voltmeter that recorded the amplitude of the spike. Telemetry outputs of the power conditioner were displayed on 0- to 5-V panel meters and also recorded digitally.

An additional testing tool was a self-contained test console procured from Hughes Aircraft Company. The performance of individual supplies was verified on dummy loads, and the response to arcing was simulated by a thyratron load. Most failures and shorts could be simulated by this unit. The test console contained instrumentation for measuring all electrical parameters and provided a convenient reference on the exact status of the power conditioner.

Table 7. Temperature sensor points

Component	Location
Thruster 1	Vaporizer
	Neutralizer
	Neutralizer tank heater
Thruster 2	Vaporizer
	Neutralizer
	Neutralizer tank heater
Thrust vector controls	Translator
	Stepper motor case
	Gimbal 1
	Differential transformer case
	Actuator base plate
	Gimbal 2
	Differential transformer case
	Actuator base plate
	Actuator cover
	Sector gear
	Saddle nut
	Stepper motor case

IV. System Integration

The system was operated to evaluate the design of various elements and to study integration problems. The in-tank portion of the test was performed in a 3×7 ft vacuum chamber maintained at a pressure of 6×10^{-6} torr. Since the system operation was maintained for lengthy intervals, sputtered material from the tank walls coating the experimental setup was a problem. A movable cover was employed to protect the nonoperating ion thruster from some of this contamination. This section provides a discussion of the operation and problems associated with the subsystems as a result of system constraints and functioning.

A. Ion Thruster

The ion thruster performance was mapped using laboratory power supplies. The output of the cathode heating supply was equipped with a 5000-Hz inverter to permit operation with the cathode transformer, which was located in the vacuum chamber near the thruster. The results of this mapping are presented in Fig. 13.

Table 8. Instrumentation electrical parameters, power conditioner

Power supply	Parameter	Indicating instrument					
		Indicating meter	Recorder, ink	Magnetic tape recorder	Digital display	Telemetry display	Oscilloscope
Magnet	I_1			X	X	X	
Vaporizer	I_2				X	X	X
Cathode heater	E_3	X					X
	I_3	X		X	X	X	
Arc	E_4		X	X	X	X	
	I_4	X	X	X	X	X	
Screen	E_5		X	X	X	X	
	I_5	X	X	X	X	X	
Accelerator	E_6		X	X	X	X	
	I_6	X	X	X	X	X	
Neutralizer heater	I_7					X	
Neutralizer keeper	E_8	X			X	X	
	I_8	X	X		X	X	
Bias	E_9	X					
	I_4	X					

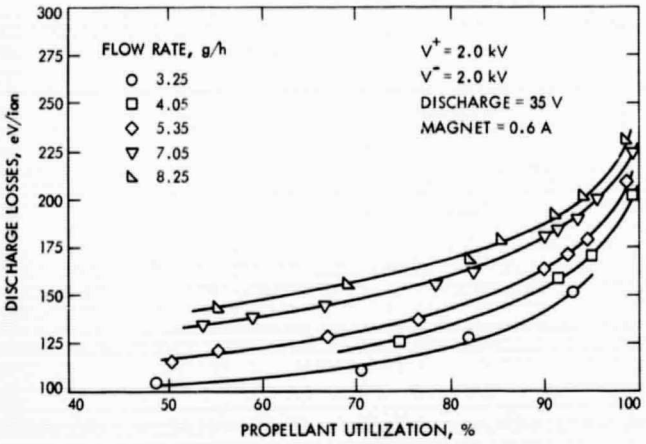

Fig. 13. Ion chamber losses as a function of utilization for various flow rates

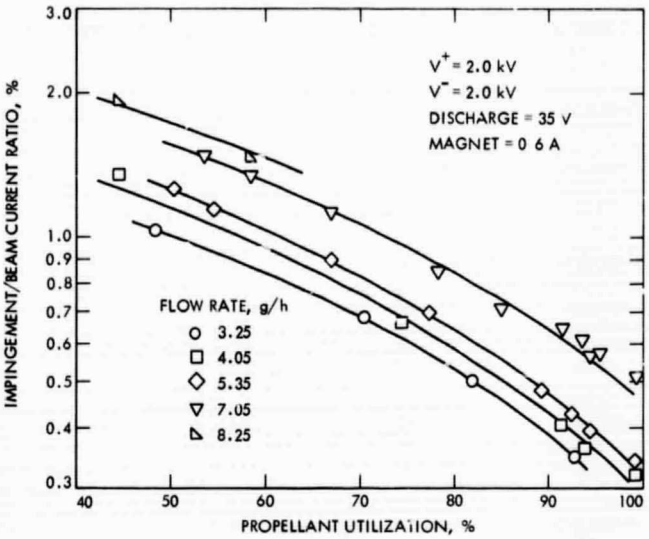

Fig. 14. Effect of propellant flow rate and utilization on accelerator impingement

where the ion chamber losses (ion chamber power/ion beam current) are presented as a function of propellant utilization (ion beam current/equivalent currents of mercury propellant flow rate) for several values of flow rate. These data, therefore, include the effects of a high-frequency cathode heating current. No unusual operational behavior was observed.

The percentage of the ion beam current intercepted by the taper accelerator grid is presented in Fig. 14 as a function of propellant utilization for several values of mass flow rate. This percentage is slightly lower than that for any on the uniform thickness grids studied in Ref. 23.

Two thruster problem areas were encountered during integration with the power conditioner. These concerned: (1) thruster performance reproducibility, and (2) transient currents during turn-on. Thruster performance variations between the two thrusters were observed as the units were operated from the power conditioner. Furthermore, high steady-state operating levels of output power were unobtainable because of large transient currents within the arc, beam, and accelerator power supplies. These currents were present within the system during reestablishing of thruster operation after the recycling of the power conditioner high-voltage supplies in response to a sustained arc between the accelerator grids. The details and approach to these two problem areas are discussed in the paragraphs that follow.

1. Thruster performance variations. Because of the unavailability of a reliable and accurate mercury flowmeter, the amount of mercury propellant used was derived indirectly from the measurement of electrical power dissipated in the ion chamber. The control of the propellant flow depended upon the ability to maintain the mass utilization at a constant value for all levels of beam current. The use of a single command for a beam reference set point was possible by employing a functional relationship to specify the arc current for each beam current level. The power conditioner was, therefore, provided with a function generator that converts the beam reference signal into an arc reference signal and reproduces a single constant propellant utilization efficiency curve (nominally 90%). Functional requirements of individual thrusters varied because of construction differences. Each thruster required its individual functional curve or a correction for thruster differences was necessary.

During ion thruster testing, it was observed that highly repeatable data generated with either the same or a similar thruster were difficult to obtain. A 5% or greater variation in discharge losses has commonly been observed during performance mapping. The similar thrusters were identical except for mechanical tolerances held during manufacture and small variations that existed in assembly. Sources of performance discrepancies that have been identified to date include: (1) small variations in electrical parameters, (2) hysteresis in the magnetic material, (3) uncertainty associated with the flow measuring technique, and (4) variations in the screen–accelerator grid geometry.

To minimize the variations in electrical parameters, the same instrumentation was used for the operation of

each thruster and power supply settings were maintained as closely as possible. Instrument calibrations were checked at frequent intervals. Operation of the power conditioner from a constant voltage power supply reduced the variations in the fixed parameters when the system functioned with this unit.

A hysteresis within the thruster permeable paths was observed. Variations from nominal (on the order of 20 G) were measured and found to be as high as 2 G. These measurements were obtained while maintaining a fixed gauss-meter position within the thruster and varying the current to the electromagnets over a wide range. In an attempt to minimize this variation, the thruster was operated at only one specified magnet current without overshoot. The observed hysteresis can be minimized to some extent by the design of the magnetic components within the thruster. The bar electromagnets employed a core constructed from a low-carbon-content magnet steel that was annealed to minimize hysteresis and maximize magnetic properties. The pole pieces used with these magnets were constructed from 1020 steel. In future tests, these pole pieces will be changed to the same core material as used for the bar magnets.

The uncertainty associated with mercury flow rate measurements was the most difficult area to resolve. The method used was to measure the rate of mercury fall within a precision bore glass tube (Ref. 24). This type of device is believed to be capable of only about 5% accuracy based on statistical data obtained over a long period of operation. Factors contributing to this accuracy are the thermal time lag of the vaporizer and connecting lines that can be very long, and can also vary considerably with the test setup. This results in some uncertainty as to the proper waiting period after each flow rate change in the flow system to stabilize. The thruster also acts as a variable heat source to perturb the setting time. Furthermore, the vacuum chamber pressure and mercury backflow from the facility can also add to the uncertainty associated with this measurement since they represent additional propellant inputs to the thruster (on the order of 3–5%).

The variations in electrical parameters and hysteresis in the thruster permeable paths could both be minimized by operating from the power conditioning unit while maintaining the input voltage at a fixed value. A repeatable, if not highly accurate, flow measurement could also be obtained during the operation of either of the two thrusters. However, variations in ion chamber performance still existed between the two thrusters.

The ion chamber performance can be affected by the ion extraction system and, therefore, constant grid geometry is critical to repeatable thruster performance. Several possible sources of error existed here. First, heating of the grids during operation could alter the grid spacing. The screen grid had been previously identified as causing this variation (Ref. 9). The supported screen grid structure used in this study presented no measurable variations in the grid gap spacing during bench tests. The ability of the grids to maintain a desired spacing was not verified during thruster operation since the present test setup did not allow for measuring of this distance. Another source of possible error arises from the fact that ion chamber losses are also functions of the screen grid open area. It follows that the mechanical tolerance of this grid should be specified closely. The tolerance used in the present study would permit 2–3% variation in the nominal open area of 70%, which could possibly result in the same order of variation in the discharge chamber losses.

The data presented in Fig. 15 show the functional relation between the arc current and the screen current over a 2:1 range of output for two nonidentical ion thrusters. The data point symbols used in Fig. 15 are defined in Table 9. The thrusters were operated from the power conditioning unit with the input voltage set at 80.0 $\pm$0.1 V, which resulted in close-setting of all electrical inputs. Each data point was held during closed-loop operation for at least 1½ h, and, after the mercury flow settled, was measured with a precision bore tube. Operating points were rechecked several days later. It was found that the functional relationship within the power conditioning unit held the mercury propellant utilization to within 4% over the entire output range for both thrusters and all grid modifications.

The differences in performance between thrusters 1 and 2 were initially found to be quite large ($\sim$15% at full power to 25% at ½ power). This difference was attributed to an inadvertently large gap (0.233 cm) that existed on the axis of thruster 1, compared to a nominal 0.178-cm gap spacing at the grid periphery. Attention was focused on the requirement for uniformity of grid separation over the entire grid area. Thruster 1 was therefore modified to approach the thruster 2 spacing. In adjusting the spacing by changing the lengths of the braces, attempts were also made to decrease the overall spacing tolerance. This was difficult because of the construction and tolerances of the thruster parts. Best results were obtained by machining a 0.25-cm deep seat for the screen grid to minimize screen pole-piece distortions.

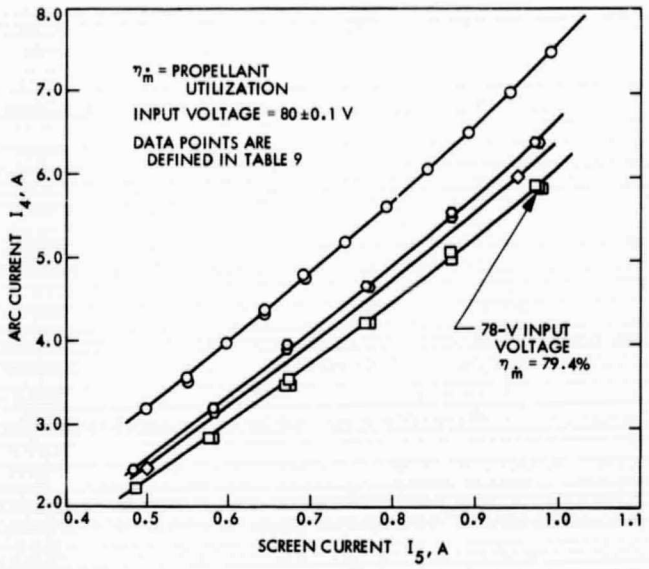

Fig. 15. Curve matching of two thrusters

After these modifications, the gap spacing better approximated that of thruster 2 and the performance was checked. A 9.9% variation in ion chamber performance was recorded, with thruster 1 showing the better performance. Variations in the gap spacing still existed between the two thrusters. Instead of striving for identical spacing on each unit, however, the nominal spacing on thruster 2 was reduced. This resulted in smaller variation between the two thrusters (about 6.0%). Since this difference did not significantly affect the system performance, no further refinements were made. The test operation satisfactorily demonstrated that the thruster performance can be trimmed to match a power conditioning unit by adjusting grid spacing.

To demonstrate the need for close control of the thruster parameters, the input-line voltage was dropped by 2.5% (2 V). For this power conditioner, this was the simplest way of varying the nonregulated outputs. This change caused a 2.5% reduction of all nonregulated outputs. Operating the thruster along the same functional curve as for the nominal line, at the point indicated in Fig. 15, resulted in lowering the propellant utilization from 83.8 to 79.4%. As the input-line voltage was decreased further (by 4 V or more, changing the unregulated outputs by 5% or more), the propellant flow could no longer be controlled and continuously increased, resulting in loss of control.

2. ***Recovery from arcing.*** In order to clear a sustained arc, the circuits in which the arc appeared were interrupted. The mechanization provided a temporary shut-

Table 9. Definition of data points in Fig. 15 for arc and beam currents

Symbol	Thruster	Grid spacing, cm		Average $\eta_{\dot{m}}$,[a] %	$\Delta\eta_{\dot{m}}$, %
		Average gap	Maximum gap		
○	1	—	0.233	93.2	±3.0
□	1	0.186	0.193	85.7	±3.0
⬡	2	0.178	0.193	86.2	±4.0
◇	2	0.168	0.178	84.0	±0.6

[a] $\eta_{\dot{m}}$ = propellant utilization.

down of the thruster to allow time to extinguish a sustained arc and for partial, if not complete, deionization of the plasma within the discharge chamber. This procedure allowed for reapplication of high voltage with no transient surge current present on the screen or accelerator supplies.

Igniting of the plasma within the thruster was observed to present high-intensity surge currents in the arc, screen, and accelerator circuits. These surges were usually higher than the protective circuitry of the power conditioner would permit. A way of minimizing these currents to present a soft start for the power conditioner was therefore sought.

The overcurrent surges were examined in detail and subsequently focused attention on the pressure within the ion chamber as the main cause of these high current conditions. The intensity of these surges has been demonstrated by changing thruster flow rates to be proportional to the ion chamber pressure. The details of the mechanism causing the pressure rise and the pressure profile with time are not presently available. A study of the interruption of the ion extraction mechanism in this continuous-flow device should provide greater insight into this phenomenon. Reduction of the ion chamber pressure, or a decrease in the density of the plasma at high-pressure conditions, are the approaches presently proposed for minimizing these surges. Some of the tests that have been run with laboratory supplies to arrive at these conclusions are described in subsequent paragraphs. These test data were obtained by interrupting thruster operation and then initiating the discharge shortly thereafter.

The ion chamber plasma density is a function of the magnetic field. Figure 16 shows how the intensity of the

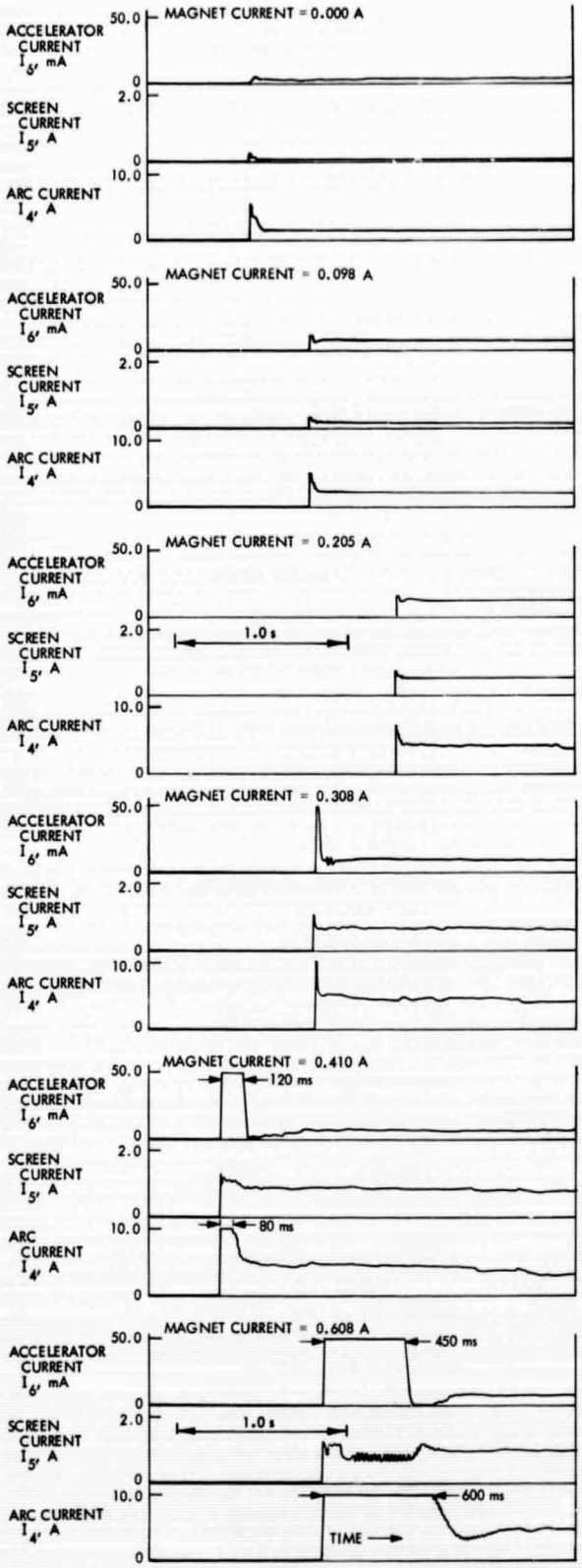

Fig. 16. Accelerator, screen, and arc currents

magnetic field (or plasma density) affects the amplitude and duration of the overshoots of the three currents from circuits that have trip limits. It became evident that the most desirable way to restart thruster operation was to do so without any magnetic field.

Ion chamber plasma density could be further reduced by decreasing either the arc voltage or current. The range of arc voltage adjustment is limited, and, therefore, only a current reduction was examined. The arc current can be reduced by lowering the cathode heating power.

In order to determine how temperature of the cathode affects the magnitude of the overshoots, the cathode power was raised from 162 W, as used previously, to 183 W, or by 13%; the mercury flow was not changed and was 9.5 g/h. Figure 17 shows the magnitude of the overshoots. Comparison of Figs. 16 and 17 shows that only marginal benefit is derived from reducing the cathode power.

The flow rate was then reduced from 9.5 to 5.77 g/h, or by 40%, and the overshoots were recorded (Fig. 18). It was evident from comparing these data with those of Fig. 16 that flow rate greatly affected the overshoots, and it was desirable to restart with a reduced rate of flow. Finally, it was also found that the rate at which the magnet current is raised can lead to undesirable overshoots (Fig. 19a). Therefore, the rate of increase of magnet current must be carefully controlled (Fig. 19b).

A minimum magnet current (about 0.075 A) and long recovery ramp were implemented within the power conditioning unit recycle procedure. This allowed system recycle over the entire output power range with acceptable transient currents present in all supplies.

Figure 20 presents the composite trace of major electrical parameters during the power conditioner recycle in response to an arc. It can be seen that as the magnet current is raised relatively slowly to the full value, the beam and arc currents recover along a smooth ramp.

B. Neutralizer

During the integration phase of the program, the neutralizer provided no operation problems with the exception of the venting valve that was found to stick frequently. The operation of the neutralizer with the thruster was mapped using the power conditioning unit.

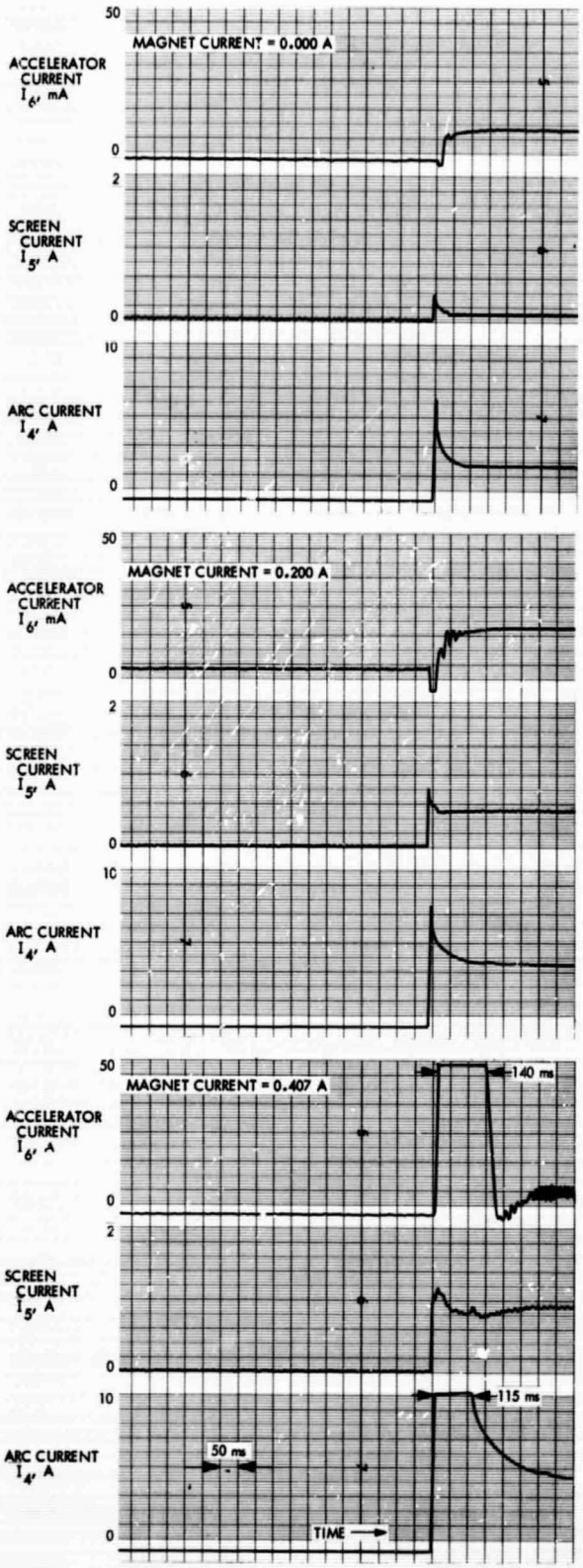

Fig. 17. Discharge initiation at high cathode power

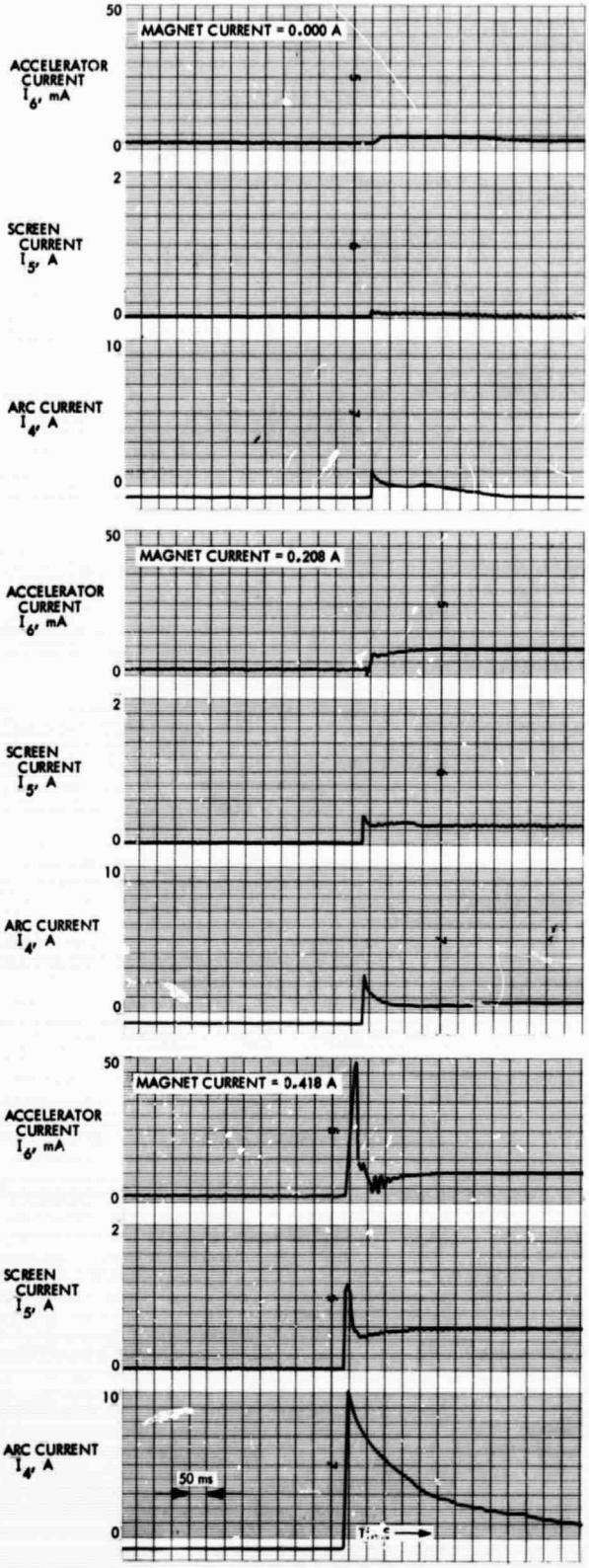

Fig. 18. Discharge initiation at low mercury flow

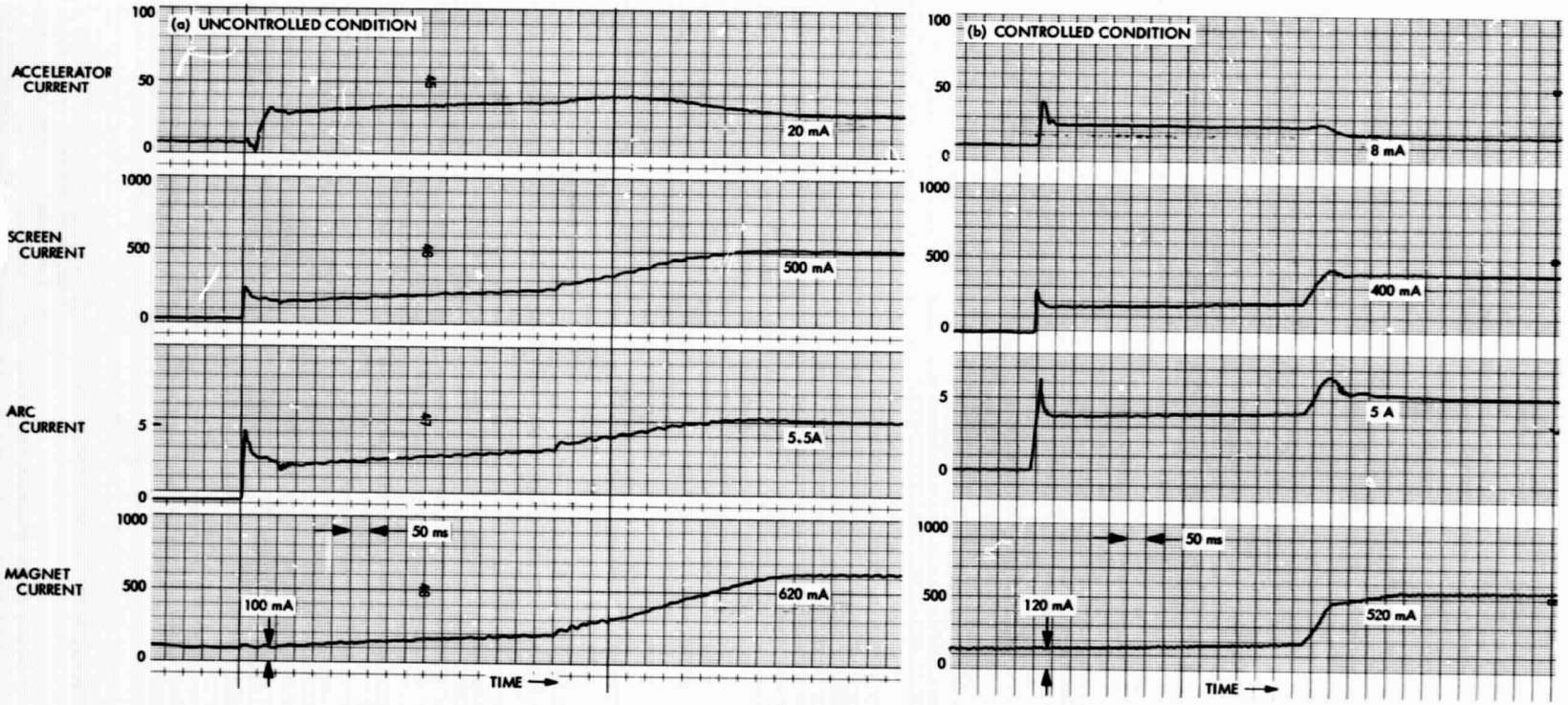

Fig. 19. Power conditioner discharge initiation as a function of magnet ramp

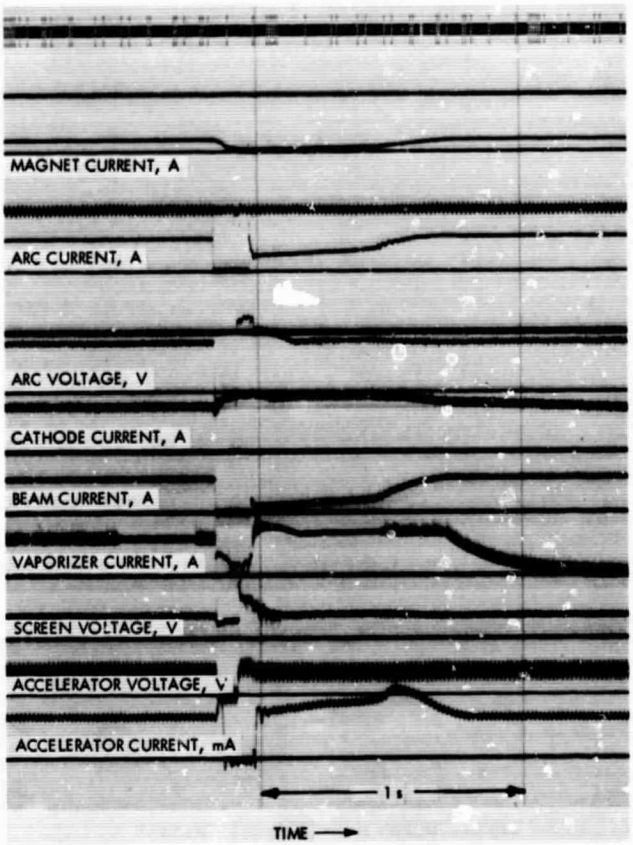

Fig. 20. Composite trace obtained during system recovery from an arc

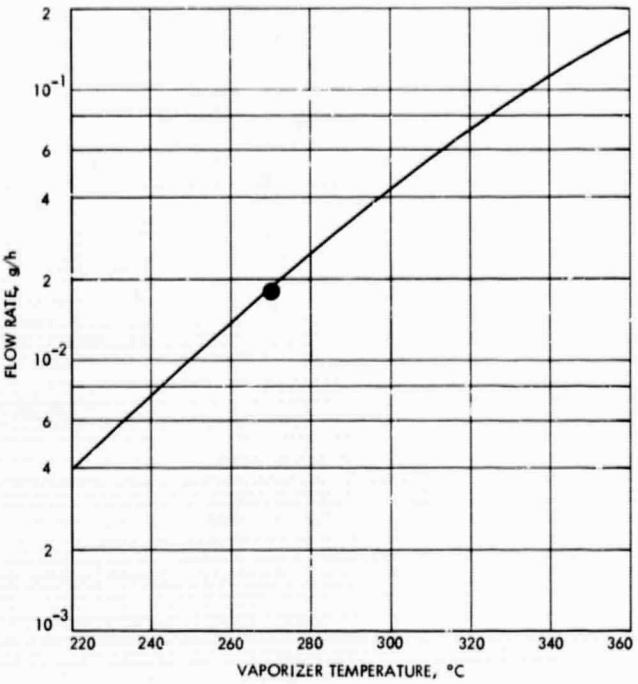

Fig. 21. Neutralizer calibration curve

The keeper voltage was maintained at a set point of 5.2 V. The cesium flow for this set point was derived from an extrapolation as presented in Fig. 21. The solid data point represents the flow rate as measured during an endurance test on this type of neutralizer at Electro-Optical Systems, Inc.* A curve was fitted through this point with the flow proportional to the vapor pressure divided by the square root of the vaporizer temperature. Flow rates derived on this basis were on the order of 0.09 g/h. The bias voltage necessary to maintain the neutralizer emission equal to the beam current as the thruster was gimballed is presented in Fig. 22 for two values of beam current. The data point values for Fig. 22 are defined in Table 10. Low voltage levels of neutralizer to beam coupling were found to exist for all values of gimbal position. These voltages were considerably below the 30-V level where detrimental wear has been observed (Ref. 16). The cesium flow was calculated to be 1.2 to 2.2% of the ion beam. No changes in the neutralizer set point were attempted at the low beam current operation. Operation of this neutralizer type with a moving beam interface yields acceptable coupling voltages and only a small penalty (~1%) in cesium flow. This performance might be improved if the set point was adjusted proportionately to the power output level.

*Personal communication with E. James, Electro-Optical Systems, Inc., Pasadena, Calif.

C. Mercury Feed

No problems were encountered with the flexible propellant lines. The latching valves exhibited a very slight leakage (0.27 g Hg/24 h at 45 in. Hg head) through the valve when in the closed position after an estimated 5000 operating cycles.

D. Power Conditioner

The power conditioner was evaluated on the test console before integration testing. The evaluation test included the measurement of the regulation characteristics of the power supplies, the verification of logic controls, and the evaluation of the operational characteristics of the control loops.

The test console was equipped with a number of special features. These included: (1) variable dummy load to verify the characteristics of each supply, (2) high-

Table 10. Definition of data points in Fig. 22 for two values of beam current

Data point symbol	Beam current, A	Neutralizer vaporizer temperature, °C	Neutralizer cesium flow, g/h	Thruster mercury flow, g/h
○	0.480	328	0.087	4.00
□	0.913	331	0.091	7.61

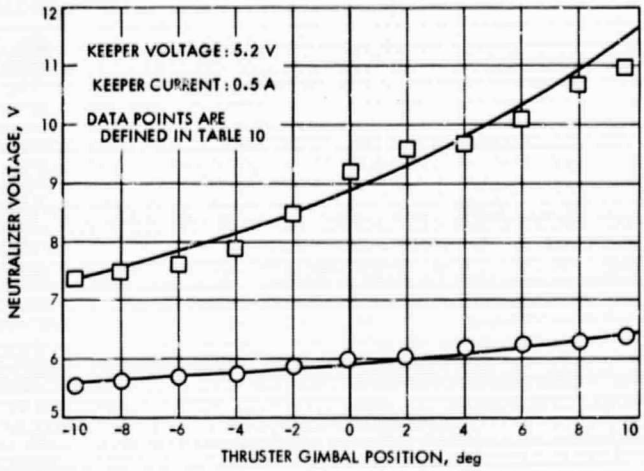

Fig. 22. Neutralizer coupling voltage as a function of thruster gimbal angle

voltage breakdown vacuum relays to check the performance of each power supply under transient conditions, and (3) digital and analog signal generation to initiate command and set the operational levels of the power conditioner control loops. Data taken during this test indicated that the power conditioning unit was 90% efficient.

The integration test with the ion thruster was initiated after the checkout of the cable connections and the installation of appropriate instrumentation to accurately evaluate and record the parameters of the power conditioner.

In the first steps of the integration test. the control loops to regulate the level of power delivered to the thruster were opened to evaluate the characteristics of each supply. Since the power conditioner was operating in open-loop mode, the level of power delivered was adjusted by variable resistors introduced in the cathode and vaporizer supplies operational amplifier. All power supplies except the neutralizer heater and keeper were connected to the ion thruster. The neutralizer heater and keeper power supplies were connected to the load on the test console. After the evaluation of the power conditioner with the ion thruster, the evaluation of the control loops was initiated.

The cathode–arc loop was initially closed while the vaporizer–screen loop was left open. The operating levels of the vaporizer supply were adjusted manually. Instability in the operation of the system was experienced with difficulty of restarting the system after interruption of sustained arc. A number of modifications were introduced to improve the characteristics of the cathode–arc closed loop. The vaporizer–screen loop was then closed. Modifications had to be introduced to overcome the restarting problems previously described. Additional modifications were also made to correct problems encountered during endurance testing.

1. Modifications. All modifications introduced during the integration tests and after the shakedown run are summarized in the listing that follows. The primary justification for these modifications was to provide stable operation and a soft restart after power conditioner recycle.

(1) The magnet supply was equipped with a delay and ramp circuit to drop the magnet current to a minimum value of approximately 75 mA with a time constant of 50 ms, maintain the minimum value during the delay time of 1 s, and ramp to the full magnet current in 0.5 s. The delay and ramp circuit was activated by the logic sensor of a sustained arc. The delay circuit was finally adjusted to provide 3 s of delay plus ramp time. To assure that magnet delay and ramp circuit were energized by the tripping logic, an OR gate was introduced. A signal input from the accelerator supply was introduced in addition to the trip sensor circuit. This arrangement produces a positive trip sensing.

(2) The overcurrent trip sensors were redesigned to slow down their response to what was considered tolerable limits. This modification was introduced to eliminate unnecessary tripping responding to an intermittent, nonsustained arcing that did not require system shutdown. The adjusted levels of overcurrent trip sensors and tripping delays for the arc current are 7.5 A, 10 ms; for the beam current, 1.09 A, 2 ms; and for the accelerator current, 106 mA, 5 ms.

(3) The gain and phase margin of the cathode–arc operational amplifier was adjusted to eliminate oscillation noticed during closed-loop operation. An open-loop gain much greater than 100 resulted in a small undamped oscillation in this loop. This result was not predicted in the analytical model of the system.

(4) A negative feedback loop was introduced in the cathode–arc operational amplifier to compensate for the true arc current sensing. The current transformer in the arc supply measured the summation of arc end beam current. To subtract the beam current, a proportional input from the beam sensing circuit was obtained and introduced in the cathode–arc operational amplifier.

(5) The vaporizer supply was equipped with a delay circuit to delay the presence of vaporizer current after an overcurrent trip for a period of 2 s.

(6) The cathode supply was equipped with a circuit to delay the presence of cathode current after an overcurrent trip for a period of 1 s.

(7) A circuit was introduced to stop the internal power conditioner clock for a period of 100–450 ms after an overcurrent trip. This arrangement assured that the high-voltage supplies would not start until after a minimum delay of 100 ms, allowing time for the magnet current to decay.

Modifications (5–7) were made after the shakedown testing of the system to correct for weaknesses uncovered in the system testing phase of the program.

2. Closed-loop servo control. From earlier theoretical studies (Ref. 21), it was found that a very close control of all electrical parameters is needed in order to retain close control of the consumption of mercury. Operation was specified in the near neighborhood of 90% mass utilization; the voltage variations were minimized by maintaining the input voltage at a fixed value.

The original loop gains (Fig. 8) for both cathode heater current–arc current and vaporizer current–screen current were measured to be approximately 250 mA. With this gain, the cathode heater–arc loop was unstable; reduction of the gain to 100 mA eliminated the condition. High gain is still desirable, however, to maintain the set point accurately. This accuracy is further decreased with time since degradation of the oxide cathode will increase the errors in the value of the arc current. The functional relation between the arc and screen currents will not be exact and the mass utilization will be affected. It is desirable, therefore, to restore the original gain of 250 mA and stabilize the operation by way of an additional phase compensation.

Typical closed-loop system operation is shown in Fig. 23. The reference set point was abruptly changed several times to indicate the response of the system. Operation of the system was completely turned off with an OFF-2 command. The system was turned on 11 min later and automatically restored normal operation. A final OFF-1 command was given that turned off only the vaporizer, allowing the thruster operation to decay.

3. Magnetic tape traces. The magnetic tape traces were a very useful tool in studying power conditioner operation while integrating the system. Typical data obtained from the magnetic tapes are presented in Figs. 20 and 24–26. Data recorded in Fig. 20 were discussed in previous paragraphs.

In Fig. 24, the arcing between screens caused a temporary shutdown. Magnet, arc, screen, and accelerator currents and screen voltage are shown to decay to zero, whereas the vaporizer current I_2 remains on. The amplitude and duration of the overcurrents in the accelerator and screen grid supplies can be identified as belonging to the nuisance category that should not trip off the system. As the blanking time was extended from the original 2 to 5 ms, the number of nuisance overcurrent trips was greatly reduced.

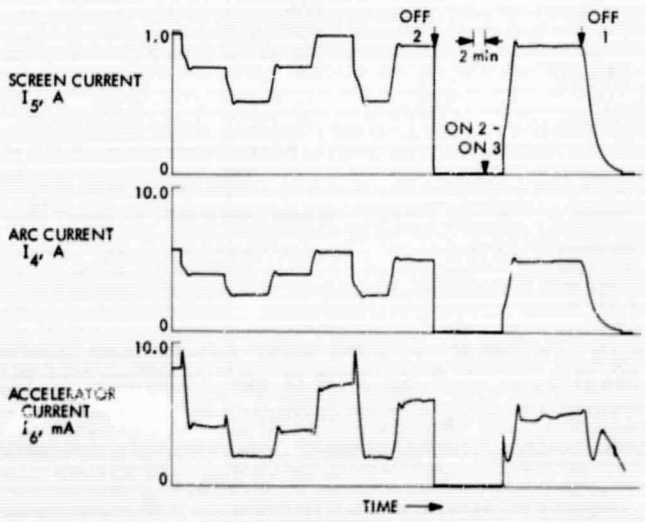

Fig. 23. Closed-loop system operation

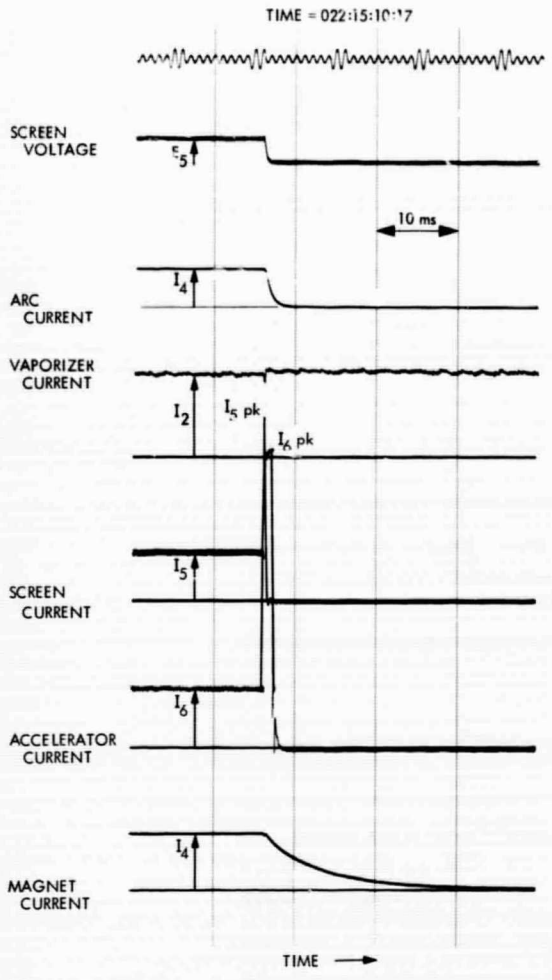

Fig. 24. Overcurrent shutdown of the system

Figure 25 traces a recycle during initial stages of recovery from arcing and indicates a large accelerator current flow during deionization of the thruster, after the power conditioner had been shut down. It also records the negative accelerator current I_6 at the time of the thruster restrike. Note the delay in striking from the time the voltages are applied. The arc, screen, and accelerator voltages (E_4, E_5, and E_6) are off for 90 ms only. In view of the fact that the magnet current requires nearly 60 ms to decay, this downtime was considered insufficient.

Figure 26 shows the downtime extended to approximately 260 ms; the arc voltage increased exponentially rather than delayed by 20 ms as originally intended. Critical currents recovered smoothly, although the magnet current ramp was shorter than the 3.5 s normal rise time. The oscillation of the screen voltage was an unresolved problem area.

4. Electrical interference. The operation of an ion thruster generates a considerable amount of interference. Even during stable operation of the thruster, with all of the regulating loops responding quickly and accurately, there is evidence of periodic arcing between various portions of the thruster. Either sustained or self-extinguishing arcs form a source of interference, the effects of which have to be minimized.

Currents changing at a high rate generate high-frequency electromagnetic fields that may induce currents in other conductors of the same harness or be picked up by various loops of wiring that act as receiving antennas. Since the magnitude of the signals generated within the receiving antenna is proportional to the area enclosed by the loop, an effort to minimize such loops was made.

All the signal grounds were attached to a single-signal ground ring that is connected to the common tie point of all the power grounds within the power conditioner. A single line connected the signal ground ring with each of the individual modules; all of the ground connections of the particular module were made to that common line.

In spite of the precautions taken, considerable noise was recorded on all dc lines inside the power conditioner logic (Table 11). In some cases, the noise levels were above the published component steady-state limits and could cause the failure of components that are exposed to them. Further clarification of transient limits and improved protection is required.

Table 11. Noise level present in power conditioner electronics

Nominal dc level, V	Location	Permissible maximum component stresses, V		Transient stresses observed, V
		Steady state	1 s	
4.5	Control	8	12	4.7
6	Control arc	8	12	8.1 8.9
	Accelerator			10.5
12	Control	18	—[a]	17.5
40	Control	100	—	57

[a]Data not available.

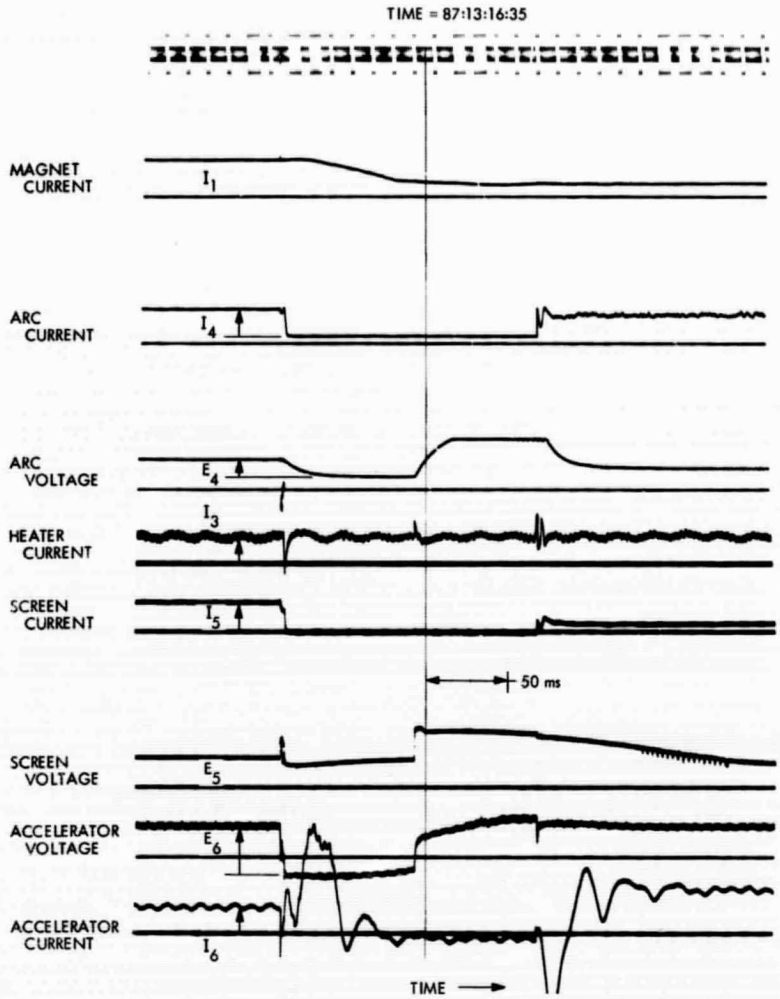

Fig. 25. System recovery from an arc

The magnitude of radiated noise may be considerably diminished by close-coupling the feed and return lines magnetically. It is felt that this was partially accomplished by inclusion of the return lines in the power harness. It is recognized that further improvements are required and could be attained by using twisted pairs and proper shielding.

In addition to being affected by radiated noise, the system performance may be affected by the conducted interference.

It was found that the overcurrent sensors inside the power conditioner were responding to an intermittent (i.e., nonsustained) arcing that did not require system shutdown. As described earlier, most of these nuisance trippings were eliminated by desensitizing the sensing circuits and slowing down their response. No tripping of the power conditioner occurred in cases where arcing was not of a sustained nature and lasted less than 5 ms.

The presence of noise generated by the plasma was evident on most of the telemetry lines. Shielding and improved grounding techniques did not help significantly because the noise was not radiated but conducted. Filtering had to be added at the input of the controller to enable processing of telemetry data without errors.

Summarizing the experiences in this area accumulated during integration testing, it can be said that electrical interference caused more trouble than was anticipated. More attention must be paid to this problem area, not only in the design of the individual subsystems, but also in the integration of the complete system.

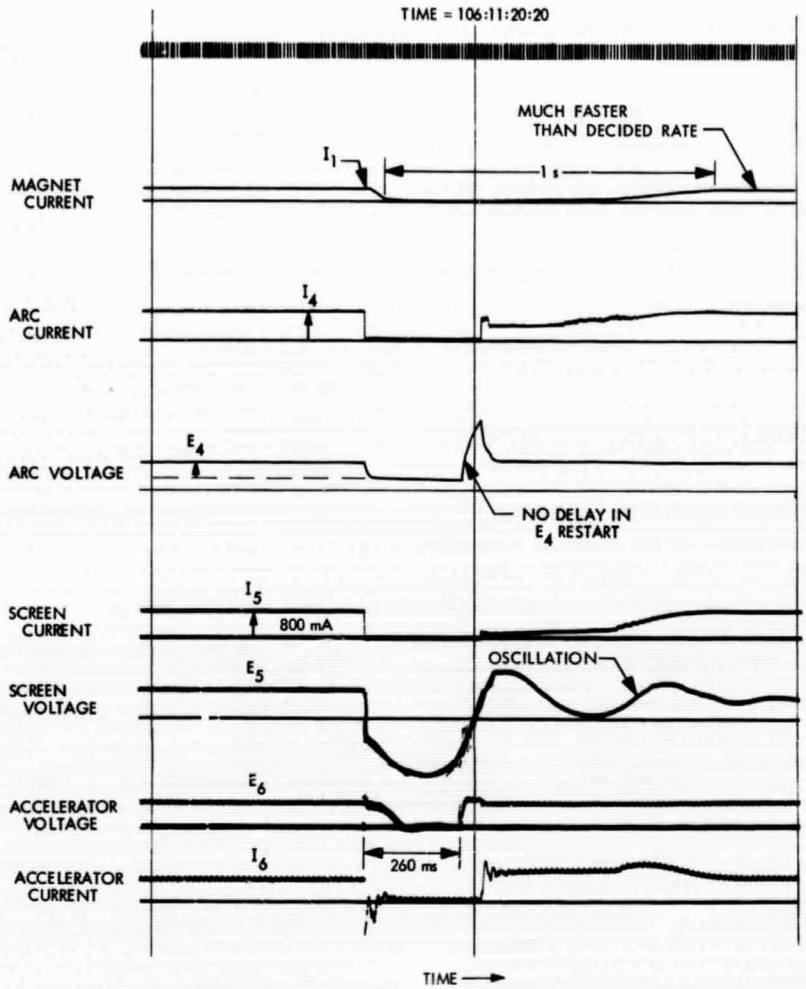

Fig. 26. Example of recovery problem areas

5. Transformer. The cathode transformer supplied with the power conditioner was mounted on one thruster and a larger transformer constructed at JPL was mounted on the second. Sputtered material proved somewhat problematical for both designs and extensive shadow shielding was required. The major problem for both transformers was the heat conducted along the leads connecting the secondary windings to the cathode. Temperatures at the transformer as high as 265°C were recorded. Redesign of the transformer to withstand higher temperatures was necessary.

E. Switching Matrix

Initial tests on the switching matrix were conducted while the controller inhibit input was negated. An artificial noise environment was introduced to examine the noise susceptibility of the unit. After these tests, the unit was installed and operated with the system. Some problems were observed during the integration test and modifications had to be introduced. These problem areas are summarized as follows:

(1) All switching was accomplished with the power conditioner turned off. The design of the power conditioner allowed the cathode voltage to be present whenever the input voltage was applied and independent of the on–off status of the power conditioner. When switching under this condition, it was possible to damage the cathode heating supply. An interlock was added between the controller and switchgear logic that prevented operation when the power conditioner input voltage was applied.

(2) The noise generated by the power conditioner and ion thruster caused the logic and position indicating

lights to malfunction. No switching of interconnections was triggered by this noise environment. Also, the commanded switching arrangements were successfully completed since the switching took place when the power conditioner and thruster were inoperative. Filter networks were introduced in the input lines of the unit to reduce the level of the noise present. With these filters in the system, the position sensors were unaffected by the system noise levels.

F. Controller

Two changes were found to be necessary when integrating the controller into the system. These were:

(1) Filters were added to the input lines to reduce noise levels. These noise levels were of sufficient intensity to affect controller operation. Initially, the noise immunity of the controller was not adequate and the failure indicating lights turned on erratically. Table 12 lists the recorded levels of noise present before filtering was added. By modifying the signal ground connections and filtering the incoming lines, the noise pickup was brought within the allowable steady-state limits and false indications were eliminated.

(2) The time during which a measured parameter was allowed to remain outside of the acceptable range was increased from 3 to 4 s to eliminate false failure indications.

G. Thrust Vector Control

During integration testing, two minor problems developed relative to the actuators. These were:

(1) A slight buckling of the gimbal actuator housing resulted in binding of this actuator, which, therefore, failed to rotate the thruster. This problem was eliminated by adding supports to the two ends of the lead screw bracket.

(2) A high leak rate was found in the gimbal cover seal where the O-ring was butted together and epoxied. This problem was eliminated by replacing the O-ring with one constructed with a vulcanized joint.

A system interaction was observed during movement of both actuators. Thruster parameters and gimbal position with time are presented in Fig. 27. The vaporizer flow rate was apparently sensitive to the system motion, suggesting a partial mercury penetration into the vaporizer or a vapor pocket in the feedline.

Table 12. Noise level present in controller critical lines[a]

Checkpoints	Steady-state level, V	Transient level, V
dc input	15	25
dc input	−15	−23
Negative reference	5.5	16
E_6 telemetry	7.4 max	17
Telemetry ground	Near zero	16

[a]All measured to chassis ground.

V. System Testing

All the problems encountered as the components were incorporated within the system have been described in the previous section. After these problems were corrected, continuous operation of the entire system became feasible. The major objectives of this continuous operation were to discover weak spots and to evaluate performance for periods longer than several hours. A shakedown run was first tried during which system faults were discovered and corrected. A final endurance test was then performed. These two tests will be described in turn.

A. Shakedown Run

1. Run profile. Several system parameters are plotted against elapsed time in Fig. 28; system events or modifications are noted.

2. Run experiences. The problems encountered are discussed in a chronological sequence in terms of elapsed time.

a. Elapsed time: 40 h. The controller was found to be damaged and the OFF-2 command driver transistor (2N2905A) had shorted. The cause of failure could not be identified. The transistor was replaced.

b. Elapsed time: 52 h. It was observed that the cathode control loop was not regulating correctly, operating at full output power continuously. This was due to the excessive power required by the cathode. The output of the cathode power supply was, therefore, increased by modifying the feedback loop characteristics of the cathode inverter. The power output was increased to 225 W,

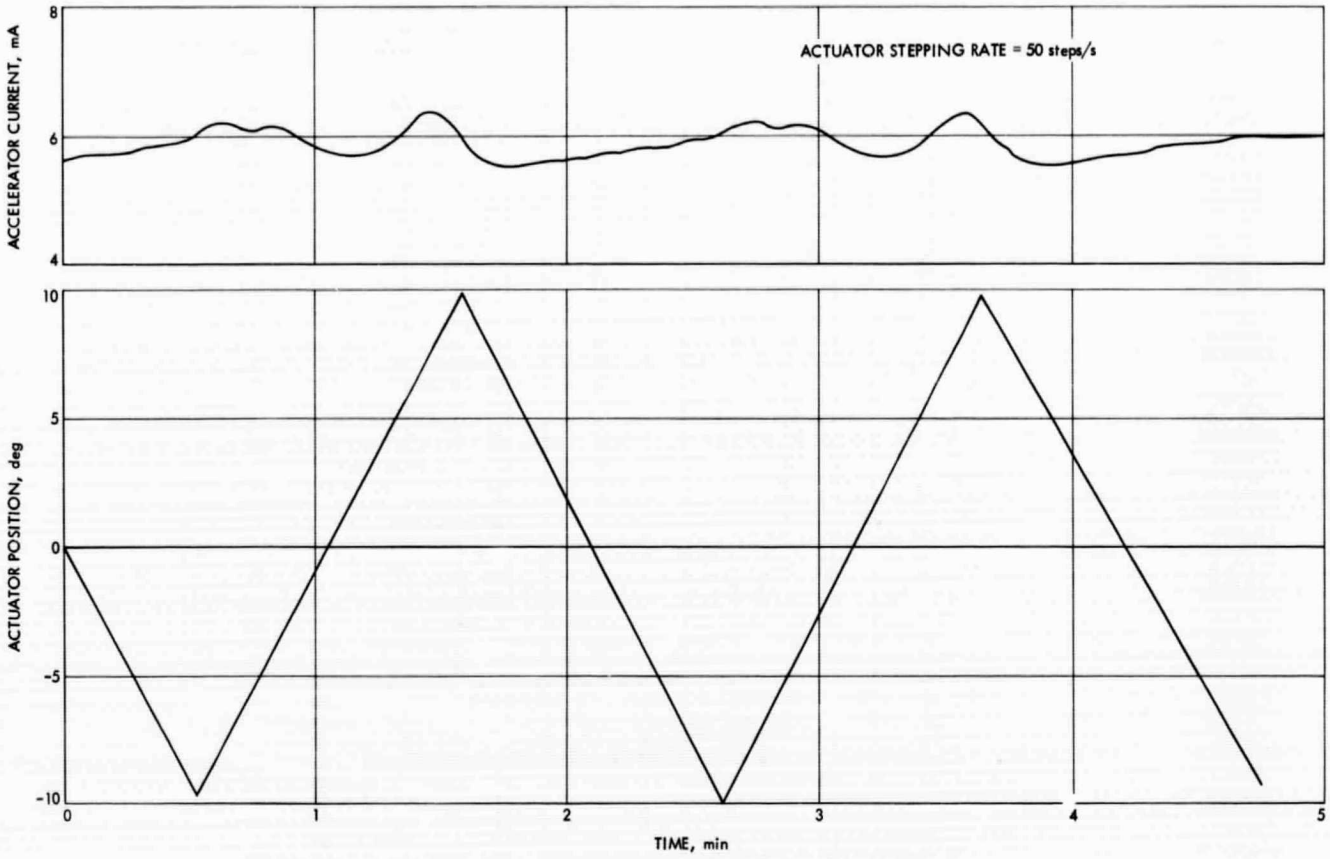

Fig. 27. Effects of actuator position on accelerator current

which is above the nominal power capability of this unit. A review of the design calculations revealed that this unit is capable of providing the required peak power; the power transistor temperature recorded after the modification verified this conclusion.

c. Elapsed time: 68 h. The operating thruster was arcing to ground excessively; recording of meaningful data became practically impossible. Operation from laboratory power supplies did not improve operation. The changeover to the spare thruster was commanded and successfully exercised by the switchgear unit. The cause of the trouble was later identified as an intermittent short between the housing of the thruster and the tank ground. The short was caused by an accumulation of sputtered material on the insulating surface. The total operation time of the system at the time of changeover was 47 h.

d. Elapsed time: 155 h. The neutralizer emission current I_E was increased from a trial setting to a value that permitted this current to match the ion beam. To increase I_E without increasing the negative bias voltage E_9 to an excessive, or lifetime-limiting, value, the flow rate of cesium in the neutralizer was increased. This was accomplished by lowering the keeper voltage E_8 from the original setting of 6 to 4.4 V.

e. Elapsed time: 168 h. The system was not capable of automatically recovering from arcing at $I_5 > 800$ mA. In order to recover, OFF-1 command had to be given, shutting down the vaporizer. After the vaporizer partially cooled, the system recovered. The ON-3 command restarted the vaporizer and the system ran until the next arcing occurred.

An attempt was made to cure the malfunction by extending the downtime of the vaporizer after arcing occurred from 100 ms to possibly 1 s or more. The quick fix was not successful and manual control of recovery had to be used.

Some malfunction inside the logic was evident because the standby units of arc and accelerator supplies were

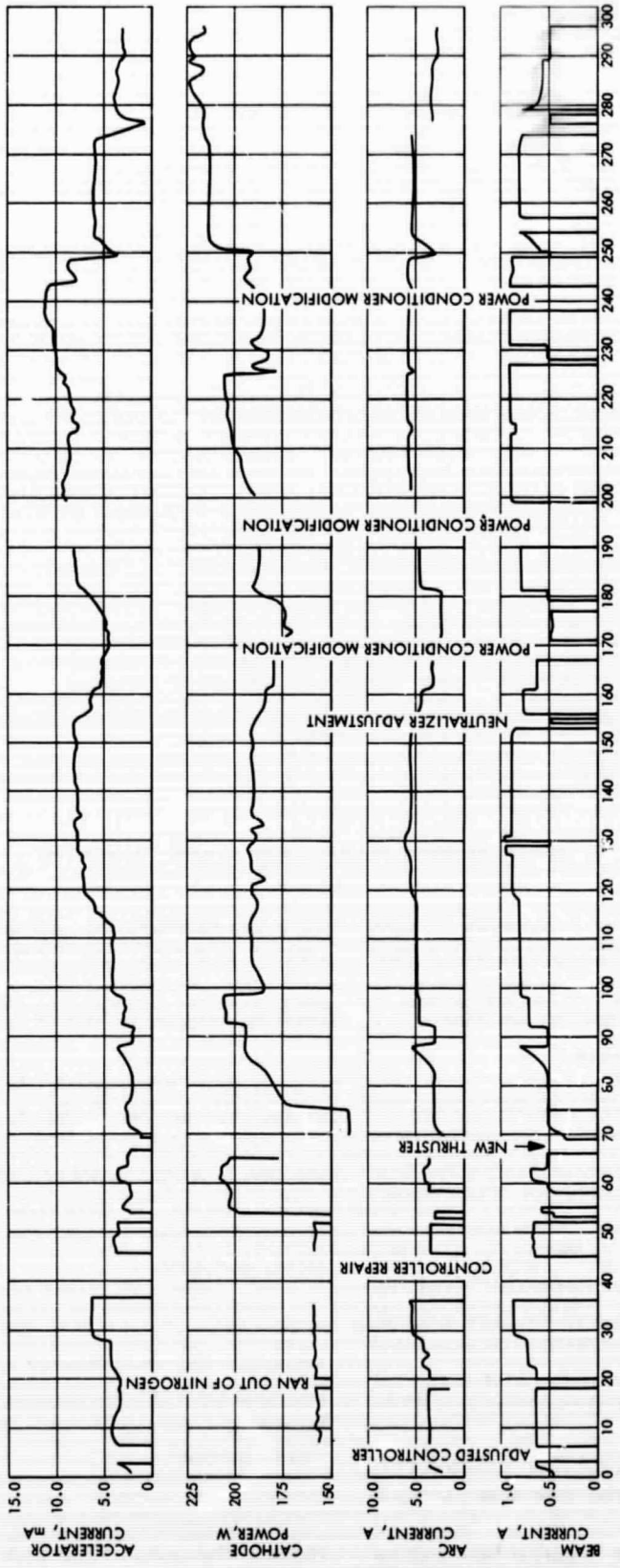

Fig. 28. Shakedown run

activated randomly, but no attempt was made to investigate at that time. Problems identified at 195 h may explain this malfunction.

f. Elapsed time: 195 h. The spare accelerator inverter logic was damaged. The failure was attributed to the fact that in some cases the magnet was not turned off after arcing, and the system tried to start with the magnets fully on, causing large overshoots (Fig. 29).

It was established that in some cases the accelerator inverter stopped running. The triggering mechanism that shuts down the magnet did not respond in time, so the system restarted with the magnet fully on.

A new trip circuit was added for the magnet that trips the magnet by the undervoltage of the accelerator power supply, rather than by overcurrent. The trouble with the magnet shutdown was corrected and the damaged accelerator inverter had to be repaired. The test was continued on the standby accelerator inverter.

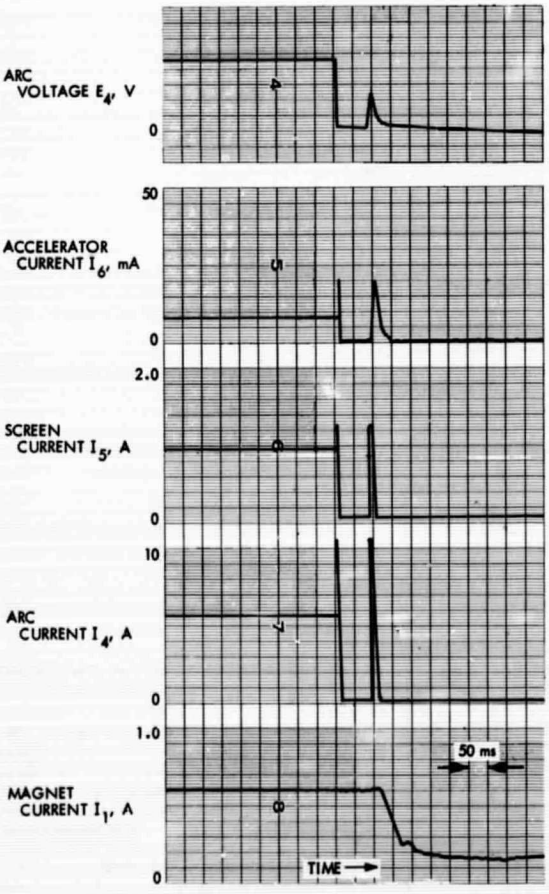

Fig. 29. Recovery from arcing

g. Elapsed time: 215 h. The step life of the stepper motor of actuator 2 was exposed to an accelerated life test. Nominal values of step life were established for the gimbal and translator actuators, based on an analysis of a Jupiter flyby mission.* A nominal 6×10^6 cycles would be required for the translator and a nominal half million for each gimbal actuator. Nominal stepping rates for the gimbal and translator actuators are 50 and 100 steps/s, respectively. Time was allotted during the shakedown test to run one gimbal approximately 13 h (2.4×10^6 steps) with one thruster on. This amply meets the design requirements. The translator and second gimbal were tested only briefly. However, all three actuators functioned normally.

h. Elapsed time: 240 h. An arc between the primary of the cathode heater transformer and the tank ground caused blowing of a protective fuse inside the power conditioner. The fuse was replaced and operation reestablished. Arcing was caused by the surface contamination of the transformer enclosure mounted inside the vacuum chamber. The method used to prevent surface contamination of that transformer was inadequate and was subsequently improved.

i. Elapsed time: 300 h. The test was stopped after 300 h. This included 252 h of actual system operation and 48 h of downtime. Table 13 lists temperatures of all critical areas of the power conditioner. No overheating of any importance was noticed. The system was capable of continued operation at this time. The inability to recycle properly at decreasing levels of beam current was the primary consideration for the termination of the test.

3. Run summary. The frequency and severity of arcing during the run were greater than the expected levels and exposed the power conditioner to a severe test, thus permitting the discovery of a number of weak links within the logic portion of the system. Despite the severe environment, the power conditioner supplies performed satisfactorily. The unit was capable of operating a clean thruster (one exhibiting a low arcing rate) at full power after the shakedown test. A detailed examination of the power conditioner after the test indicated that a power transistor in an arc inverter had failed. Several loose wires were also found within the logic system. The system was operating on the standby arc inverter.

**1975 Jupiter Flyby Mission Using Electric Spacecraft,* Advanced Studies Document 760-18. Jet Propulsion Laboratory, Pasadena, Calif., Mar. 1968.

Table 13. Temperatures measured in the power conditioner

Sensor location	Temperature, °F
Screen inverter	134
Line regulator	128
Arc inverter	102
Accelerator inverter	98
Cathode inverter	98
5-kHz inverter	89

Problems encountered during shakedown testing arose from several sources. These included: (1) weakness in power conditioner logic, (2) power conditioner rework, (3) sputtered material within the vacuum facility, and (4) plasma properties causing intense surge currents. Each of these problem areas is discussed in the paragraphs that follow.

The weakness in the power conditioner logic was symptomized by the random restart of the high-voltage supplies (accelerator, screen, arc). In the design tested, these supplies were started by pulses generated in the logic clock. After a temporary shutdown of the supplies during thruster arcing, the presence of the first clock pulse started the accelerator supply, followed by the screen and arc supplies. The time of restart after shutdown varied from zero to the maximum clock pulse duration of 350 ms. A delay in restart of 100 ms minimum was necessary to accomplish the interruption of a sustained arc. It was felt that the random restart feature was not acceptable, and this deficiency was corrected.

It must also be pointed out that the light weight of the power conditioner made it very susceptible to mechanical damage. In a number of cases, connections were broken off due to the extensive rework this unit has been subjected to both in the past and during the present program. Quality control inspection and procedures would be helpful in eliminating this problem area.

Some of the problems uncovered during the shakedown run resulted from the large amount of surface contamination inside the vacuum tank. The exposed surfaces were coated to a thickness varying between 0.001 and 0.003 cm and the accelerator grid was contaminated with metallic flakes. Although protected, the cathode transformer suffered from some surface coating and was intermittently arcing from terminals to ground.

It was recognized early in this program that the vaporizer power should be reduced during periods of repetitive recycling. This feature was lacking, however, during shakedown testing, and, therefore, many of the system shortcomings were compounded.

Modifications were incorporated within the power conditioner to correct the problems experienced and improve the characteristics of recovery after a temporary shutdown. These included:

(1) A circuit was introduced to stop the clock for a period of 100 to 450 ms after a temporary shutdown occurred. This arrangement will assure that the high-voltage supplies will start after a minimum of 100 ms.

(2) A 2-s vaporizer shutdown has been included to eliminate the overheating of the vaporizer during repeated breakdowns.

(3) A 1-s reduction in cathode power to 25 A was also felt to be desirable since the upper limit on cathode power has been raised. The reduction protects the cathode from excessive temperature during the recycle procedure.

A revised recycle sequence after a temporary shutdown caused by thruster arcing was, therefore, developed. The sequence is shown in Table 14.

B. Endurance Test

1. Run profile. The thruster arc current, screen current, and cathode heating power are plotted against

Table 14. Restart sequence after a temporary shutdown

Time	Sequence of events
Zero	Arc, screen, or accelerator current exceeds limit. PS 4, PS 5, and PS 6 are turned off. Magnet and vaporizer currents are reduced to a minimum value within 100 ms. Cathode current is reduced to 25 A
100 to 450 ms	Screen and accelerator voltages are reapplied. Arc voltage ramped up within 20 ms
700 ms to 1.5 s	Discharge initiated. Arc, screen, and accelerator currents self-establish
1 s	Cathode current released to 40 A
2 s	Vaporizer current released to maximum value
2.5 s	Magnet current ramp is initiated
3.0 s	Magnet current reaches final value

system operating time in Fig. 30. The system was operated at decreasing power levels with time to demonstrate power matching capabilities. After reaching the lowest power level of interest, the system was again increased to full power. The run was terminated after 298 h of operation. System events are noted on the run profile figure.

2. *Run experiences.* Problems encountered and changes introduced are discussed in chronological sequence in terms of operating time. The system began operation with thruster 2 connected to the power conditioner.

a. Elapsed time: 18 h. The arc current was observed to be too high. Operation was switched to thruster 1 to determine whether a thruster or power conditioner problem existed. System operation was essentially unchanged with the second thruster. The function generator was believed to be set for too high a value of propellant utilization. Long-term mercury measurements were taken to verify this conclusion.

b. Elapsed time: 34 h. The gimbal actuator on thruster 1 was turned on and set to operate continuously at a rate of 50 steps/s.

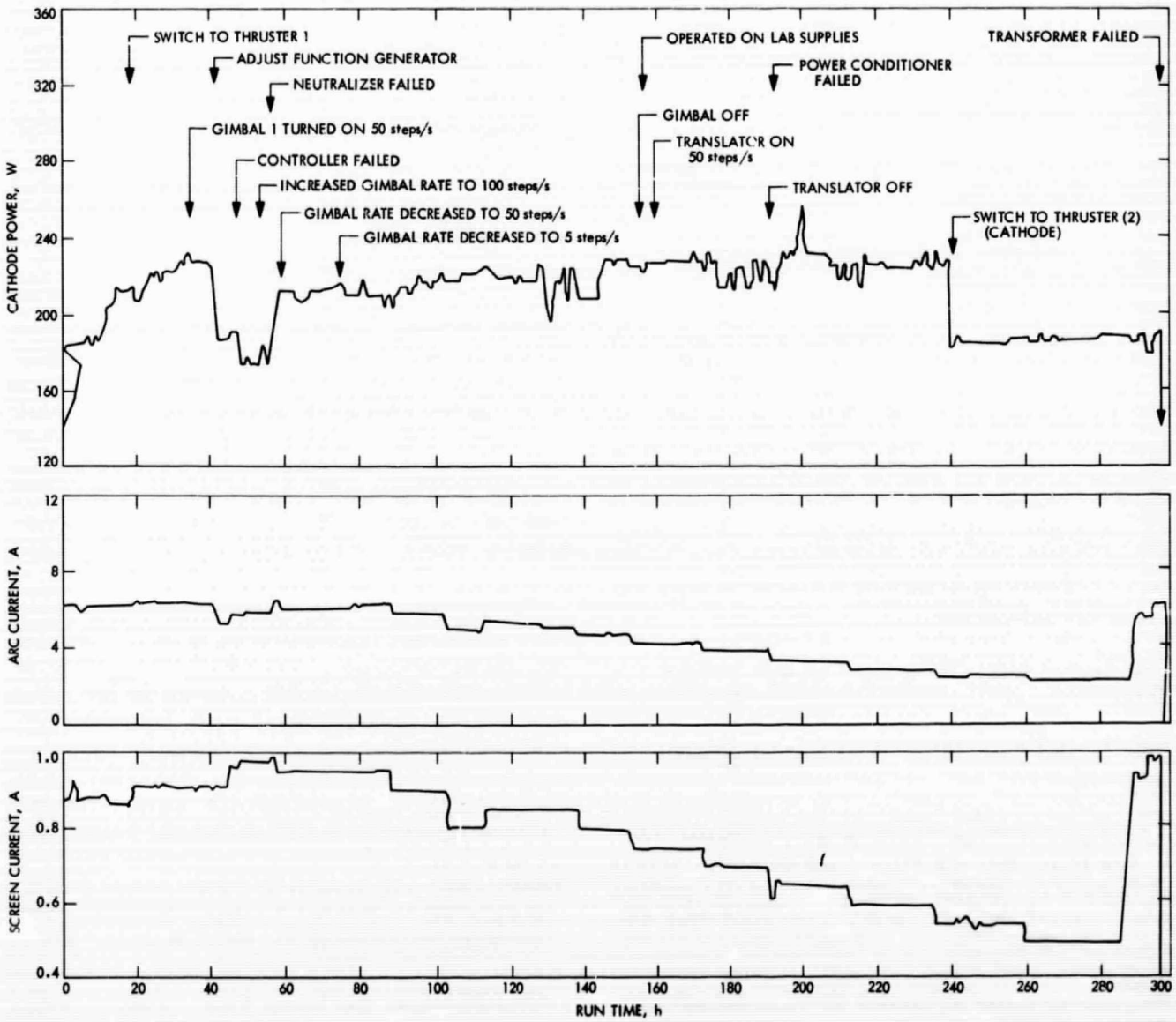

Fig. 30. Endurance run

c. Elapsed time: 41 h. Long-term propellant measurement indicated the system was operating at a high level of propellant utilization. The function generator within the power conditioning unit was set (screwdriver adjustment) to operate closer to the desired 90% utilization.

d. Elapsed time: 47 h. The controller failed. The OFF-2 command driver transistor shorted again. Power conditioner command was switched to the test console for the remainder of the test.

e. Elapsed time: 56 h. The neutralizer failed. A hole was noted on the stem of the neutralizer that connected the vaporizer to the cathode. This allowed cesium to escape and a plasma to seat at this location. The power conditioner neutralizer outputs were connected to dummy loads for the remainder of the test. Gimbal 1 stepping rate was increased to 100 steps/s.

f. Elapsed time: 59 h. Gimbal 1 stepping rate was decreased to 50 steps/s.

g. Elapsed time: 74 h. Gimbal 1 stepping rate was decreased to 5 steps/s.

h. Elapsed time: 155 h. Gimbal 1 was turned off. A sufficient number of steps had been accumulated.

i. Elapsed time: 156 h. The thruster was switched to laboratory supplies and operated for several hours in an attempt to clean up some of the surface buildup of sputtered material that was believed to be responsible for the excessive system recycling rate. The average hourly rate of system recycling during the 24-h period before and after operating with laboratory supplies was reduced from 32 to 18.

j. Elapsed time: 159 h. The translator actuator was turned on and set to operate continuously at 50 steps/s.

k. Elapsed time: 191 h. The translator actuator was turned off.

l. Elapsed time: 192 h. The power conditioner failed. It was found that the main accelerator inverter was shorted and the standby would not turn on. The problem was traced to a shorted transistor in the main accelerator supply shutoff circuitry and a damaged transistor in the starting circuitry of the accelerator standby unit. The damaged parts were replaced. A filter network was introduced in the switching relay circuitry of the main and standby units to eliminate chattering during switching from main to standby units. This chattering could possibly have caused the failure of the starting transistor in the standby unit. The failure of the shutoff transistor in the main accelerator inverter was considered a part failure. During the repair of the main and standby accelerator units, a number of power transistors in the screen inverters were shorted as the result of an error during the checkout procedure with dummy loads. Damaged parts were replaced and a modification was made to provide an additional time delay between the arc supply main and standby units. The delay circuit was introduced at the switching relay.

m. Elapsed time: 240 h. Thruster 1 failed. The cathode heating current would no longer heat the cathode to the desired operating temperature. Operation was switched to thruster 2. The problem was later found to be condensed sputtered material shorting the cathode leads.

n. Elapsed time: 298 h. The transformer on thruster 2 opened up on the secondary side because of excessive operating temperatures.

3. Run summary. The frequency of arcing during the run was decreased by about 50% over that experienced during the shakedown run by the addition of more intricate shadow shields at each problem area where severe sputtered material buildup was observed. The rate of system recycle in response to arcing averaged 20–30 cycles/h. Sputtered material coatings remained a problem and were responsible for the failure of thruster 1 where one side of the cathode was shorted to the thruster body.

The failure of the neutralizer was believed to be the result of a localized chemical attack of the stainless steel and was a consequence of the neutralizer handling procedures rather than the design, inasmuch as this type of neutralizer has functioned satisfactorily for several thousand hours (Ref. 25). In the described test, the neutralizer was exposed to atmosphere in the intervals between runs. The neutralizer was backfilled with argon before this exposure. Diffusion of oxygen through the orifice and a chemical reaction of cesium at the vaporizer surface of the nickel wick were possible. It is believed that products of this reaction could have been responsible for oxidation of the neutralizer body that was observed at this location.

Controller failure was believed to be a result of system noise. A more detailed investigation of the noise signals and a redesign of the line filters appear to be necessary.

Additional weaknesses were uncovered in the accelerator portion of the power conditioner that were not discovered during the shakedown run. There was also evidence of the power conditioner logic being affected by the noise levels. Several OFF-2 commands were internally generated by the noise during the endurance run. When this occurred, manual commands were immediately given to restore system operation.

The actuators performed satisfactorily during the test. Leak rate tests were performed on the gimbal actuator prior to system testing and after 250 and 550 h. The results, which are summarized in Table 15, indicate a leak rate within specifications with no significant increase with time.

Table 16 summarizes the cycle test results for all three actuators. Included are the calculated number of cycles required for a Jupiter flyby mission. As can be seen in the table, all actuators met and, in the cases of the gimbal actuators, significantly surpassed the total cycle requirement.

VI. Conclusions

An experimental investigation was conducted on the system aspects of solar electric propulsion. The system was successfully integrated and endurance tested over a time period that totaled 550 h of actual operation. The total number of operating hours on the power conditioner, including integration testing, was on the order of 1,000 h, during which time the unit was recycled nearly 10,000 times in response to thruster arcing. Essentially few problems existed in the power portion of the power conditioner; most were found within the logic. The maximum demonstrated lifetime of the power conditioner and each of the other system components is listed in Table 17. The actuators were the most successful components tested, meeting lifetime requirements. Severe facility limitations, in the form of backsputtered material from the vacuum tank walls when stopping the high velocity ion beam, prevented long thruster lifetimes and also presented a strenuous power conditioner evaluation by causing excessive thruster arcing. Sputtered material coated all electrical connections and insulators, requiring excessive shadow shielding. The thruster cathode could not be shielded, and this eventually resulted in the failure of thruster 1.

The light weight of the power conditioner unit and the excessive number of modifications during the described and previous programs reduced the quality of the unit substantially. However, system noise was the major lifetime-limiting factor for both the power conditioner and controller.

Table 15. Gimbal actuator leak rates

Component	Leak rate, scc[a]/h (90% N_2, 10% He)		
	Prior to test	After 250 h	After 550 h
Gimbal actuator 1	5.5×10^{-3}	2.7×10^{-3}	7.4×10^{-3}
Gimbal actuator 2	4.0×10^{-3}	3.8×10^{-3}	4.5×10^{-3}

[a]scc = standard cubic centimeters.

Table 16. Endurance test total steps accumulated—actuators

Component	Mission requirements, steps	Accumulated in test, steps
Translator actuator	$< 6.35 \times 10^6$	8.30×10^6
Gimbal actuator 1	$< 6.35 \times 10^5$	12.125×10^6
Gimbal actuator 2	$< 6.35 \times 10^5$	2.40×10^6

Table 17. Maximum component lifetimes obtained during system testing at JPL

Component	Exhibited lifetime during system testing, h	Major lifetime limitation
Ion thruster	220	Facility sputtering (metal coating)
Neutralizer	114	Improper handling procedures
Controller	220	System noise
Power conditioner	195	System noise
Gimbal actuator	121 (12.12×10^6 steps)	None encountered
Translator actuator	32 (8.30×10^6 steps)	
Actuator electronics	200	
Switchgear	1000 (500 estimated operations)	
Switchgear electronics	600	
Latching valve	— (5000 estimated cycles)	None encountered

The conclusions derived as a result of system integration and testing are as follows:

(1) The discharge chamber power of an ion thruster, necessary to provide a specified output power and propellant utilization, may be adjusted to some extent by modifying the gap spacing between accelerating grids. This adjustment allows slightly different thrusters to be trimmed so as to give identical operation from a given power conditioning unit.

(2) The use of an ion thruster employing electromagnets provides system advantages. Control of the thruster magnetic field provided convenient control of the plasma density within the discharge chamber, permitting a soft restart of the system. This restart procedure minimized transient overcurrents observed to be present during both initiation of a discharge and sudden changes in the strength of the magnetic field.

(3) Closed-loop control of a system was demonstrated for a continuous 2:1 range of output power, while maintaining propellant utilization in the neighborhood of 90%.

(4) Electrical interference generated by the ion thruster and power conditioner was found to be a source of integration problems. This interference was reduced to a tolerable level by introducing line filters and shielding, and by minimizing the area of all loops that could serve as receiving antennas. The levels of noise inside the electronic circuits were not compatible with high-reliability requirements and long-term degradation may be expected. This limitation could be eliminated by designing proper noise protection into the logic system.

(5) Short-term endurance of shakedown system testing with a thruster exhibiting a high rate of arcing is an effective method for detecting system weaknesses. In this type of environment, power conditioner weaknesses are rapidly discovered, providing a form of accelerated system life testing.

The testing of a solar electric propulsion system has uncovered several real and potential problem areas. Some of these will require further investigation. No fundamental limitations were uncovered. However, it is felt that with a reduction in backsputtered material (e.g., by the use of a larger vacuum facility) and with system electronics constructed of high-reliability components and with noise immunity designed in, then system lifetime compatibility with the flight requirements could be achieved.

References

1. Barber, T. A., and Meissinger, H. F., "Simplification of Solar Electric Propulsion Missions by a New Staging Concept," AIAA Paper 69-251, presented at the AIAA Seventh Electric Propulsion Conference, Williamsburg, Va., Mar. 3–6, 1969.

2. Schwaiger, L., Molitor, J. H., and MacPherson, D., "Spacecraft Designs for Multipurpose Solar Electric Propulsion Missions," AIAA Paper 69-252, presented at the AIAA Seventh Electric Propulsion Conference, Williamsburg, Va., Mar. 3–6, 1969.

3. Stract, W. C., and Zola, C. L., *Solar Electric Propulsion Probes for Exploring the Solar System*, TM X-52318. National Aeronautics and Space Administration, Cleveland, Ohio, 1967.

4. Macie, T. W., et al., "Solar Electric Propulsion System Evaluation," AIAA Paper 69-498, presented at the AIAA Fifth Propulsion Joint Specialist Conference, U. S. Air Force Academy, Colorado Springs, Colo., June, 1969.

5. Pawlik, E. V., Macie, T. W., and Ferrera, J. D., "Electric Propulsion System Performance Evaluation," AIAA Paper 69-236, presented at the AIAA Seventh Electric Propulsion Conference, Williamsburg, Va., Mar. 3–6, 1969.

6. Ferrera, J. D., and Perkins, G. S., "Actuator Development for a Clustered Ion Engine Array," in *Supporting Research and Advanced Development*, Space Programs Summary 37-54, Vol. III, pp. 60–63. Jet Propulsion Laboratory, Pasadena, Calif., Dec. 31, 1968.

7. Ferrera, J. D., and Pawlik, E. V., "Actuator Endurance Testing for a Clustered Ion Engine Array," in *Supporting Research and Advanced Development*, Space Programs Summary 37-58, Vol. III, pp. 129–131. Jet Propulsion Laboratory, Pasadena, Calif., Aug. 31, 1969.

8. Pawlik, E. V., "Neutralization of a Movable Ion Thruster Exhaust Beam," in *Supporting Research and Advanced Development*, Space Programs Summary 37-58, Vol. III, pp. 211–215. Jet Propulsion Laboratory, Pasadena, Calif., Aug. 31, 1969.

9. Masek, T. D., "Evaluation of the SE-20C Thruster Design," in *Supporting Research and Advanced Development*, Space Programs Summary 37-51, Vol. III, pp. 124–128. Jet Propulsion Laboratory, Pasadena, Calif., June 30, 1968.

10. Masek, T. D., and Pawlik, E. V., "Hollow Cathode Operation in the SE-20C Thruster," in *Supporting Research and Advanced Development*, Space Programs Summary 37-53, Vol. III, pp. 120–123. Jet Propulsion Laboratory, Pasadena, Calif., Oct. 31, 1968.

11. Hyman, J., Jr., et al., "Liquid-Mercury Cathode Electron-Bombardment Thrusters," AIAA Paper 69-302, presented at the AIAA Seventh Electric Propulsion Conference, Williamsburg, Va., Mar. 3–6, 1969.

12. *Ion Engine Thrust Vector Study*, Quarterly Report No. 1 on JPL Contract. Hughes Aircraft Company, Malibu, Calif., Apr. 1968.

13. Pawlik, E. V., and Reader, P. D., *Accelerator Grid Durability Tests of Mercury Electron-Bombardment Ion Thrusters*, NASA TN D-4054. National Aeronautics and Space Administration, Washington, D.C., July 1967.

References (contd)

14. Sohl, G., Fosnight, V. V., and Goldner, S. J., *Electron Bombardment Cesium Ion Engine System*, Summary Report on NASA Contract CR-54711, Report 6954. Electro-Optical Systems, Inc., Pasadena, Calif., Apr. 1967.

15. *Evaluation of Electric Propulsion Beam Divergence and Effects on Spacecraft*, Second Quarterly Letter, NAS 7-575. TRW Systems Group, Redondo Beach, Calif., Jan. 20, 1968.

16. Rawlin, V. K., and Pawlik, E. V., "A Mercury Plasma-Bridge Neutralizer," paper presented at the AIAA Electric Propulsion and Plasmadynamics Conference, Colorado Springs, Colo., Sept. 1967.

17. *Development and Test of an Ion Engine System Employing Modular Power Conditioning*, Project Final Report SSD-60374-R. Hughes Aircraft Company, Culver City, Calif., Sept. 1966.

18. Elder, F., and Staley, L. E., *An Experimental Model of a 2kw 2500v Power Converter for Ion Thrusters Using Gate Controlled Switches in Two Phase Shifter Parallel Inverters*, NASA Report CR 54216. Wilmore Electronics Company, Inc., Durham, N.C., May 17, 1965.

19. Ernsberger, G. W., *An Experimental Model of a 2kw 2500v Power Converter for Ion Thrusters Using Silicon Transistors and a Pulse-Width-Modulator Bridge Inverter*, NASA Report CR 54217. Wilmore Electronics Company, Inc., Durham, N.C., Mar. 1, 1965.

20. Moore, E. T., Wilson, T. G., and McIntire, J. N., *Development of a 1.6kw 2000v, High Frequency ac–dc Converter for Ion Thrusters Using a Modular Design and an Inductive Energy Pumping Technique for Conversion, Regulation and Protection*, NASA Report CR 54408. Wilmore Electronics Company, Inc., Durham, N.C., Dec. 8, 1965.

21. Mueller, P. A., and Pawlik, E. V., "Control Analysis of an Ion Thruster with Programmed Thrust," AIAA Paper 69-239, presented at the AIAA Seventh Electric Propulsion Conference, Williamsburg, Va., Mar. 3–6, 1969.

22. Costogue, E., "Electric Propulsion Power Conditioning," in *Supporting Research and Advanced Development*, Space Programs Summary 37-51, Vol. III, pp. 35–36. Jet Propulsion Laboratory, Pasadena, Calif., June 30, 1968.

23. Masek, T. D., and Pawlik, E. V., "Thrust System Technology for Solar Electric Propulsion," AIAA Paper 68-541, presented at the AIAA Fourth Propulsion Joint Specialist Conference, Cleveland, Ohio, June 10, 1968.

24. Eckert, A. C. et al., *Investigation, Testing, and Development of an Electron-Bombardment Ion Engine System*, NASA Contract NAS3-5745, TRW Final Report ER-6291. TRW, Cleveland, Ohio, Dec. 1964.

25. Fosnight, V. V., et al., "Cesium Ion Engine System Life Test Results," *J. Spacecraft Rockets*, Vol. 5, No. 4, Apr. 1968.

NASA — JPL — Coml., L.A., Calif.